

國立交通大學

機械工程學系

碩士論文

Preliminary Experimental Investigation of a DC Gas

Discharge With and Without Magnetron System

以實驗的方式初探在有無磁控管系統的直流電漿源氣體放電情況

研究生：梁偉豪

指導教授：吳宗信 博士

中華民國九十五年七月

以實驗的方式初探在有無磁控管系統的直流電漿源
氣體放電情況

Preliminary Experimental Investigation of a DC Gas Discharge With and
Without Magnetron System

研 究 生：梁偉豪

Student : Wei-Hao Liang

指導教授：吳宗信博士

Advisor : Dr. Jong-Shinn Wu

國 立 交 通 大 學
機 械 工 程 學 系
碩 士 論 文



**Submitted to Institute of Mechanical Engineering Collage of
Engineering**

National Chiao Tung University

In Partial Fulfillment of the Requirements

for the degree of

Master of Science

In

Mechanical Engineering

July 2006

Hsinchu, Taiwan, Republic of China

中華民國九十五年七月

致 謝

在交大求學的這兩年來，感謝吳宗信老師悉心教導，讓我無論是在學習過程中或是生活上都成長許多，在研究及做學問方面，因為老師不厭其煩的教導，而使我的成長許多也學到許多，處理事情以及解決問題變得更有效率，並且也充實了我許多日常生活經驗，感謝老師這些日子以來的照顧。同時也感謝口試委員傅武雄教授、魏大欽副教授在口試時提供的寶貴意見，使得本論文更加充實完備，在此一併致謝。

實驗室的氣氛融洽，使得我在良好的學習環境學習，學習過程中更有效率。感謝學長(姐)邵雲龍、李允民、周欣芸、洪捷榮、許哲維、鄭凱文在研究上及生活上的教導及幫助，感謝同學育進、孟樺、百彥在學習上的相互切磋砥礪，以及學弟們生活上的幫助與鼓勵，使我這兩年的研究生活非常充實且溫馨，並能夠順利完成學業。

此外，感謝在交大這二年的生活中陪伴著我的各位好友以及我的家人，有你們的鼓勵，使得我更能堅持下去。在這離別的季节裡，大家各奔前程，去追求自己心中的夢想。希望大家在不久的將來，我們都能擁有屬於自己的一片天空。

梁偉豪 謹誌

九五年七月于風城

以實驗的方式初探在有無磁控管系統的直流電漿源

氣體放電情況

學生：梁偉豪

指導教授：吳宗信 博士

國立交通大學機械工程學系

摘 要

近幾十年來，電漿在半導體工業的運用越來越廣泛。其中直流電漿源可以用簡單的機制使得氣體能夠輕易的產生輕微的解離而形成電漿，並且直流電漿源被普遍的運用在濺鍍金屬材料來形成薄膜沉積方面已經有很好的例子。

如果就直流放電的電漿，其電漿產生所需達到的崩潰電壓根據帕申(Paschen)曲線，當氣體解離所需要達到崩潰電壓一般都需要相當高的氣體壓力。但這在這壓力下，離子或分子的平均自由徑卻相當的小，要使得被轟擊出來的原子能夠黏著在基材上也就相當不容易。所以為了要使直流電漿源能夠操作在較低的壓力下，一般比較常見的作法會在靶材附近增加磁場，利用磁力來限制從靶材轟擊出來的二次電子，用以增加在靶材附近的電漿密度。

此研究最主要的目的就是要了解電漿參數的變化，所以我們會利用蘭牟耳探針(Langmuir probe)深入電漿內部，來量測電漿內的電漿特性變化，並比較在有無外加磁場的情況下電漿特性的改變。

Preliminary Experimental Investigation of a DC Gas Discharge With and Without Magnetron System

Student : Wei-Hao Liang

Advisor : Dr. Jong-Shinn Wu

Department of Mechanical Engineering
National Chiao Tung University

Abstract

In the recent years, the field of gas discharge plasma applications has rapidly expanded in semiconductor industry. The dc discharges has been applied in generating weakly ionized plasmas and has been studied the properties of plasma. The dc glow discharges have been used as the sputtering source to product thin film and other specialized application for a long time.

As illustration in the Paschen curve, the pressure that discharges exceed breakdown voltage must be high enough ($p > 30\text{mTorr}$) and maintain in the usually manner by the secondary electron emission from the cathode. These pressures are higher than the optimum for deposition of sputtered atoms onto the substrate. This results in sputtered atom poor adhesion for the sputtered film. It is desirable to operate a sputtering discharge at lower pressures than to be obtained in a conventional glow discharge. This has led to the use of a dc

magnetic field at cathode to confine the secondary electrons.

This research will use Langmuir probe to measure the properties of dc discharges in the condition with and without magnetron and compare the difference between this two conditions.



INDEX

致 謝	I
摘 要	II
ABSTRACT	III
INDEX	V
LIST OF TABLE	VII
LIST OF FIGURES	VIII
CHAPTER 1 INTRODUCTION.....	1
1.1 BACKGROUND AND MOTIVATION	1
1.2 PLASMA SOURCES AND DIAGNOSTICS.....	3
1.3 LITERATURE SURVEY	5
1.3.1 <i>The Development of Diagnostic Theory</i>	5
1.3.2 <i>Applications of DC Sputtering System</i>	7
1.4 OBJECTIVES AND ORGANIZATION OF THE THESIS.....	9
CHAPTER 2 EXPERIMENTAL APPARATUS	11
2.1 EXPERIMENTAL FACILITY	11
2.1.1 <i>Overview of the DC-magnetron sputtering system</i>	11
2.1.2 <i>Pressure gauges</i>	11
2.1.3 <i>Plasma source</i>	12
2.1.4 <i>Magnetron assembly</i>	13
2.1.5 <i>DC Power Supply</i>	13
2.2 EXPERIMENTAL INSTRUMENTATION	13
2.2.1 <i>Langmuir probe</i>	13
2.2.2 <i>Thermocouple</i>	14
2.3 EXPERIMENT METHODS AND STEPS	15
CHAPTER 3 LANGMUIR PROBE DIAGNOSTICS.....	16
3.1 TYPICAL <i>I-V</i>	16
3.2 THEORY OF LANGMUIR PROBE.....	18
3.2.1 <i>Planar Probe with Collisionless Sheath</i>	19
3.2.2 <i>Cylinder probe with collisionless sheath</i>	23
3.3 THEORY OF ELECTRON ENERGY DISTRIBUTION FUNCTION (EEDF)	25
3.4 PARAMETER CALCULATION	28
CHAPTER 4 RESULTS AND DISCUSSION	30

4.1 THE DISCHARGES WITH MAGNETRON	30
4.1.1 Plasma potential and floating potential.....	31
4.1.2 Plasma density	32
4.1.3 Electron temperature.....	34
4.2 THE DISCHARGES WITHOUT MAGNETRON	35
4.2.1 Plasma potential and floating potential.....	36
4.2.2 Plasma density	37
4.2.3 Electron temperature.....	37
CHAPTER 5 CONCLUSIONS AND FUTURE WORK.....	39
5.1 SUMMARY.....	39
5.2 RECOMMENDATIONS FOR FUTURE WORK	40
REFERENCE	41



List of Table

Table 1. The value of $(V_p-V_f)/T_e$ in different places in the chamber with working pressure 30 mtorr and operated with magnetron.....	85
Table 2. The value of $(V_p-V_f)/T_e$ in different places in the chamber with working pressure 20 mtorr and operated with magnetron.....	85
Table 3. The value of $(V_p-V_f)/T_e$ in different places in the chamber with working pressure 10 mtorr and operated with magnetron.....	86
Table 4. The value of $(V_p-V_f)/T_e$ in different places in the chamber with working pressure 70 mtorr and operated without magnetron	86
Table 5. The value of $(V_p-V_f)/T_e$ in different places in the chamber with working pressure 80 mtorr and operated without magnetron	87



List of Figures

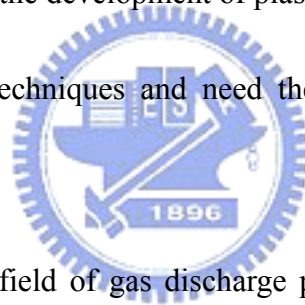
Figure 1.1. Breakdown voltages in various gases for the plane parallel electrode [Raizer, 1991]..	44
Figure 1.2. Construction of a cylindrical probe	44
Figure 2.1. The DC-magnetron Sputtering System	45
Figure 2.2. The MKS self-tuning controller	45
Figure 2.3. The Baratron capacitance manometer	46
Figure 2.4. The Wide-Range Vacuum Gauge Controllers	46
Figure 2.5. The ion gauge	47
Figure 2.6. The thermocouple gauge.....	47
Figure 2.7. The plasma source	48
Figure 2.8. The Magnetron System	48
Figure 2.9. The LakeShore 421 Gaussmeter.....	49
Figure 2.10. The DC power control panel.....	49
Figure 2.11. Standard ESP analysis system with motorized Z-motion control	50
Figure 2.12. RF-compensated probe	50
Figure 2.13. Automatic Z-motion drivers	51
Figure 2.14. The position of thermocouple in the chamber.....	51
Figure 2.15. Schematic of experimental chamber.....	52
Figure 3.1. Typical <i>I-V</i> curves for Langmuir probe.....	53
Figure 3.2. Qualitative behavior of the sheath and presheath in contact with a wall.....	53
Figure 3.3. Ion orbital motion within the sheath of a cylindrical Langmuir probe	54
Figure 4.1. The coordinate in the chamber where the origin is on the center of the target surface. (a) the coordinate is on the picture (b) the coordinate is on the schematic of experimental chamber	55
Figure 4.2. The discharge was operated with the magnetron assembly in the pressure 10 mtorr .	56
Figure 4.3. The horizontal distribution of plasma potential in the pressure 30 mtorr and the distance between substrate and target is (a) 11 cm and (b) 8 cm.	57
Figure 4.4. The horizontal distribution of plasma potential in the pressure 20 mtorr and the distance between substrate and target is (a) 11 cm and (b) 8 cm.	58
Figure 4.5. The horizontal distribution of plasma potential in the pressure 10 mtorr and the distance between substrate and target is (a) 11 cm and (b) 8 cm.	59
Figure 4.6. The horizontal distribution of floating potential in the pressure 10 mtorr and the distance between substrate and target is (a) 11 cm and (b) 8 cm.	60
Figure 4.7. The horizontal distribution of floating potential in the pressure 20 mtorr and the distance between substrate and target is (a) 11 cm and (b) 8 cm.	61
Figure 4.8. The horizontal distribution of floating potential in the pressure 30 mtorr and the distance between substrate and target is (a) 11 cm and (b) 8 cm.	62

Figure 4.9. The vertical distribution of floating potential in the horizontal position $x=-2$, $x=0$ and $x=2$ and working pressure in (a) 30, (b) 20 and (c) 10 mtorr.....	64
Figure 4.10. The difference of plasma density difference between <i>OML</i> and EEDF; the working pressure is (a) 30, (b) 20 and (c) 10 mtorr.	65
Figure 4.11. The horizontal distribution of plasma density in the distance 11 cm between the substrate and the target. The working pressure is (a) 10, (b) 20 and (c) 30 mtorr.....	67
Figure 4.12. The horizontal distribution of plasma density in the distance 8 cm between the substrate and the target. The working pressure is (a) 10, (b) 20 and (c) 30 mtorr.....	68
Figure 4.13. The vertical distribution of plasma density in the horizontal position $x=-2$, $x=0$, $x=-2$ and $x=4$ and working pressure in (a) 10, (b) 20 and (c) 30 mtorr.....	70
Figure 4.14. The horizontal distribution of electron temperature in the distance 11 cm between the substrate and the target. The working pressure is (a) 10, (b) 20 and (c) 30 mtorr.....	71
Figure 4.15. The horizontal distribution of electron temperature in the distance 8 cm between the substrate and the target. The working pressure is (a) 10, (b) 20 and (c) 30 mtorr.....	73
Figure 4.16. The difference of electron temperature between sheath theory and EEDF; the working pressure is (a) 30 and (b) 20 mtorr.....	74
Figure 4.17. The vertical distribution of electron temperature in the horizontal position $x=-2$, $x=0$, $x=-2$ and $x=4$ and working pressure in (a) 10, (b) 20 and (c) 30 mtorr.	76
Figure 4.18. The changes of electron temperature in the different working pressure and in the same vertical position $z=4$	77
Figure 4.19. The discharge was operated without the magnetron assembly in the pressure 90 mtorr	78
Figure 4.20. The horizontal distribution of plasma potential in the distance between substrate and target is 4 cm and working pressure (a) 70 mtorr and (b) 80 mtorr.....	79
Figure 4.21. The horizontal distribution of floating potential in the distance between substrate and target is 4 cm and working pressure (a) 70 mtorr and (b) 80 mtorr.....	80
Figure 4.22. The horizontal distribution of plasma density in the distance between substrate and target is 4 cm at working pressure (a) 70 mtorr and (b) 80 mtorr and (c) the distance between substrate and target is 5 cm at working pressure 70 mtorr.	82
Figure 4.23. The horizontal distribution of electron temperature in the distance between substrate and target is 4 cm at working pressure (a) 70 mtorr and (b) 80 mtorr and (c) the distance between substrate and target is 5 cm at working pressure 70 mtorr.	84

Chapter 1 Introduction

1.1 Background and Motivation

Advances in microelectronics technology over the last two decades have exceeded even the most optimistic expectations. It depends on the application of plasma, i.e. etching, deposition, sputtering, surface cleaning, ion implantation and diamond film, etc. in semiconductor industry. We should know the circumstance of plasma first and then we will know the design of the plasma source could meet our needs or not. When talking to the development of plasma sources, it is quite important to improve the diagnostics techniques and need the knowledge of mechanism to generate plasma.



In the recent years, the field of gas discharge plasma applications has rapidly expanded. This is due to the large chemical freedom offered by non-equilibrium aspects of the plasma. This wide variety of chemical non-equilibrium condition is possible, since (external condition) parameters can be modified, such as:

The chemical input (working gas; this defines the different species in plasma: electrons, atoms, molecules, ions, etc.)

The pressure (ranging from 1 mTorr to atmospheric pressure; as mentioned above, a higher pressure typically reduces the confinement and pushed the plasma toward equilibrium)

The electromagnetic field structure (typically externally imposed, but it can also be modified by the plasma species; these electric and magnetic fields are used to accelerate, heat, guide and compress the particles.)

The discharge configuration (*e.g.* with or without electrodes; discharge volume)


The temporal behavior (*e.g.* pulsing the plasma)

In dc discharge, a few electrons are accelerated by the electric field in front of the cathode; collide with the gas atoms and cause excitation and ionization. The ionization collisions create new electrons and ions. The ions are accelerated by the electric field toward the cathode, where they release new electrons by ion induced secondary electron emission. The electrons give rise to new ionization collisions, creating new ions and electrons. These processes of electron emission at the cathode and ionization in the plasma make the glow discharge self-sustaining plasma.

The pressure is an important factor to reach the breakdown voltage in the dc discharge and the minimum value of breakdown is relative to electrode distance and pressure (Figure 1.1). These pressures are higher than optimum for deposition of sputtered atoms onto the substrates due to scattering of sputtered atoms by argon atoms. The sputtering efficiency of a dc discharge can be improved by a hollow cathode. However the geometry also becomes a limiting factor for deposition, leading

to the addition of a magnetic field. It is clearly desirable to operate a sputtering discharge at higher current densities, lower voltages, and low pressures than can be obtained in a conventional glow discharge. This has led to use of a dc magnetic configuration. The permanent magnet placed at the back of the cathode target generates magnetic field lines that enter and leave through the cathode plate. The magnetic field could trap the electrons near the cathode in order to achieve the intention had been mentioned above.

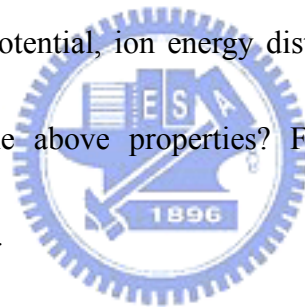
1.2 Plasma Sources and Diagnostics



There are various ways of transferring energy from fields to plasma discharges. Utilizing different electron heating mechanism, it would influence the characteristics of the plasma, i.e., capacitive discharges, inductive discharges, wave-heated discharges and dc discharges. Capacitive discharges have been the most widely used source for low-pressure materials processing. However, the limitation of capacitive RF discharges and their magnetically enhanced variants have led to the development of various low-pressure, high-density plasma discharges, i.e., inductively coupled plasmas (ICP) and electron cyclotron resonance (ECR), etc. Besides preceding plasma sources, a dc discharge has one obvious feature, its macroscopic time independence that is simpler than RF discharges. The dc discharge has been historically important,

both in application of weakly ionized plasma and in the studying the properties of the plasma medium. DC discharge is also a fine source to begin plasma diagnostic technique.

After introduction to the plasma sources briefly, we would be interesting in the plasma properties. The purpose to diagnose is appreciating the basic plasma properties and further we can control the fabrication of semiconductor devices to detect the quality of the process of deposition and etching, etc. The basic plasma properties that we are interesting are plasma density, electron temperature, electron energy distribution, plasma potential, ion energy distribution and floating potential, etc. How do we receive the above properties? Following will introduce some diagnostics techniques shortly.



The diagnostics techniques could be generally divided into invasive and non-invasive diagnostics techniques. The invasive diagnostics include microwave diagnostics and optical methods. Each of above methods has different application ways, i.e. interferometer, plasma induced emission spectroscopy, laser induced fluorescence (LIF) and absorption spectroscopy, etc. All of these methods are generally measure the entire averaged properties of the plasma. The invasive diagnostics include Langmuir probe and emissive probe and the invasive diagnostics can do localized diagnosing. Although invasive diagnostic, like Langmuir probe,

would make perturbation in the plasma, it's still a good studying tool. The Langmuir probe specially can obtain more plasma properties than other diagnostic techniques and its price also has a small advantage than others.

1.3 Literature Survey

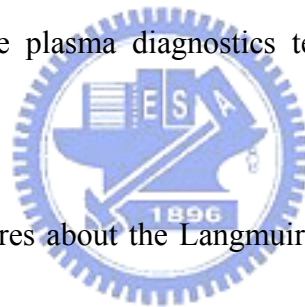
1.3.1 The Development of Diagnostic Theory

One of the fundamental techniques (the first one, in fact) for measuring the properties of plasmas is the use of electrostatic probes. This techniques was developed by Langmuir and Mott-Smith [Langmuir and Mott-Smith, 1926] as early as 1924 and consequently is sometimes called the method of Langmuir probes, basically an electrostatic probe is merely a small metallic electrode, usually a wire, inserted into plasma. The probe is attached to a power a supply capable of biasing it at various voltages positive and negative relative to the plasma, and the current collected by the probe then provides information about the condition in the plasma.

In 1950s, many scientists [Schneider, 1956; Boyd and Twiddy, 1959] proved that the electron velocity distribution is not completely complying with Maxwellian velocity distribution and not completely isotropic especially in low pressure, partially ionization plasma. Druyvesteyn [Druyvesteyn, 1930; Druyvesteyn and Warmoltz,

1935] successfully proved, in 1930, any type of Electron Energy Distribution Function (EEDF) could be directly received by the secondary differential of the $I-V$ curve of the probe. And EEDF could be employed directly to calculate the plasma properties.

Johnson and Malter [Johnson and Malter, 1949, 1950] developed double probes in 1949 and Yamamoto [Yamamoto and Okuda, 1956; Okuda and Yamamoto, 1960] improved to triple probe in 1960. The triple probe measurement replaced the sweeping bias method used in the single and double probe measurement. Both of above development make the plasma diagnostics techniques more selectivity and comprehensive applications.



There are lots of literatures about the Langmuir probe in the plasma diagnostic techniques, and F. F. Chen [Chen, 1965] in 1965 gathered all of the literatures about Langmuir probe together to supply the completely analyzing in all kind of modules and theories. Except Chen, Swift, Schwan [Swift, 1971] and Schott [Schott, 1995] supplied large contribution in the integrated of probe diagnostics techniques and analysis methods.

Laframboise [Laframboise, 1966] especially do the discussion of the theory and study to the spherical and cylindrical probe, and get the practical and important result. The following scholars mostly quote his results to the investigation and application of

the probe.

From 1924, Langmuir introduced the electrostatic probe to plasma diagnose, it allowed people to understand the phenomenon in the plasma. Langmuir probe still applies to the design and development of high density plasma source today.

1.3.2 Applications of DC Sputtering System

DC planar magnetron discharge are widely and maturely used for sputtering deposition metallic thin films such as aluminum, zincoxide, gold, and various alloy and have gained wide acceptance for high rate deposition of blanket metal films with good film adhesion. A permanent, electromagnet, or rotating magnet assembly is often used in the magnetron to confine energetic electrons. With the applied magnetic field, the ionization efficiency is effectively increasing so that high deposition rate could be achieved at a relatively low pressure.

In 1985, Rossnagel and Kaufman [Rossnagel and Kaufman, 1986] used Langmuir probe to character the plasma properties of a magnetron sputtering system. Langmuir probe presented to investigate more close to the cathode region. The experiment presented the plasma sheath thicknesses were estimated from the potential variations for the low-current discharge and compared the plasma potential, electron temperature and electron density in different pressures. S. Z. Wu [Wu, 2005] set up

and investigated a discharge in dual-side dc magnetron system in 2005, and he explored the detail correlation between plasma density and discharge parameters. The power input and gas pressure are two major parameters to tune the deposition process. In Wu's study it was shown that as these two parameters are varied, discharge characteristic change correspondingly.

Pulsed-mode, non-continuous and continuous are two plasma systems have widely used for plasma-based processes. Pulsed dc magnetron sputtering technology has been developed in the last 10 years as useful tool for deposition of high-quality dielectric thin films. Typically, these sputtering sources are operated in the frequency range from 10 to 100 kHz and the duty cycles from 50% to 90% with two operation methods of the unipolar and bipolar modes. The characteristics of plasma during pulses and between pulses are very important in plasma-based processes as well as understanding plasma physics.

Seo [Seo *et al.*, 2005] investigated the effect of the duty cycle of the cathode pulse on the plasma parameters in the pulsed magnetron discharges of constant-voltage mode, constant-power mode and constant-current mode. They observed that as the duty cycle of the pulse is reduced, the average electron rapidly increases irrespective of the operating mode, although the average electron density strongly depends on the operating mode. They also expected that a high-voltage pulse

operation with a short duty cycle can produce the high-temperature plasma that yields improved films quality by achieving a high ionization rate of the sputtered atoms. The time-resolved Langmuir probe technique has been developed to obtain the evolution of the characteristics of the plasma versus time during high-voltage pulses and between pulses. However, the secondary electron emission during high-voltage pulses seriously interferes with plasma measurement. Qin and McTeer [Qin and McTeer, 2005] used a time-delayed and time-resolved Langmuir probe measurement to measure the evolution of the plasma densities versus time of a dc pulsed, non-continuous plasma.



1.4 Objectives and Organization of the Thesis

The purpose of the present study is to use Langmuir probe to obtain the plasma properties in the sputtering system. It will show the investigation of the plasma with and without the magnetron assembly and apply in different theory ways, i.e. sheath theory and electron energy distribution function method. And then we would construct plasma diagnose the plasma properties of the system and to make the plasma diagnostic becomes simple in the future.

The organization of the thesis would be stated as following. It would start from introduction and introducing the experimental apparatus briefly. The analysis theory of Langmuir probe will be expounded carefully. The results and discussions will be

obtained by the theories introduced in the following chapter. It would finally show the summarization of the thesis and the recommendation for the future work.



Chapter 2 Experimental Apparatus

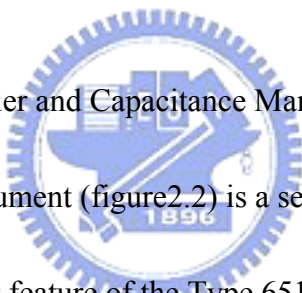
2.1 Experimental Facility

2.1.1 Overview of the DC-magnetron sputtering system

The figure 2.1 shows overview of the dc-magnetron sputtering system that contains unit of mass flow controller, system control panel, valve controller, pressure gauge, dc power control panel and the chamber.

2.1.2 Pressure gauges

1. MKS Pressure Controller and Capacitance Manometer



The MKS Type 651 instrument (figure 2.2) is a self-tuning pressure controller for throttle valves. The self-tuning feature of the Type 651 unit determines system characteristics necessary for control. This feature takes into account time constants, transfer functions of the valve and plumbing, valve gain, pump speed, and many other important parameters when determining the system characteristics. The default window display on the front panel shows the pressure readout and the valve position (% open). The pressure readout can be displayed in units of Torr, mTorr, mbar, μ bar, Pascal, or kPa. Five reprogrammable set points are provided, each one having the option of being setup for pressure or position control. Valve open, close, and stop functions are also provided on the front panel for use in system setup and diagnostics.

The instrument has a high-powered driver to operate MKS type throttle valves and equip with Baratron transducers (Capacitance Manometer figure2.3) giving the unit a control range from 10^{-3} to 0.1 Torr.

2. Thermocouple Gauge and Ion Gauge

The Model 934 Wide-Range Vacuum Gauge Controllers (figure2.4) provide pressure measurements across a broad range of vacuum environments. It also provides easy-to-use, intuitive front panel and large, bright, digital displays for ion gauge and low-vacuum gauges. The Model 934 controller connected to a single Bayard-Alpert ion gauge (figure 2.5) covers a pressure range that formerly required two instruments. It allowed us to set gas factor in vacuum gauge controller to display corrected readings if our system uses different gases. The gas factor is a multiplier that the vacuum gauge controller applies to a reading before it shows the result on the digital ion gauge display. The working range of the ion gauge is from 2×10^{-10} Torr to 1 Torr. The low-vacuum gauge is thermocouple gauge (figure 2.6) and the working range of the thermocouple gauge is from 10^{-3} Torr to 999 Torr.

2.1.3 Plasma source

The figure2.7 shows the top view in the chamber and we can find in the central

figure is the cathode region that we provide negative voltage source. And it is our target in the centre of the picture that was made by aluminum.

2.1.4 Magnetron assembly

The figure 2.8 shows the top view and side view of the magnetron system. The magnetic field is provided by a magnet assembly consisting of a diameter of 8.3 cm iron plate on which is mounted a series of 1.1x0.6x2.6 cm magnets (see figure 2.8) with the entire assembly mounted vertically under the target. The magnetic field was measure by the Lakeshore 421 Gaussmeter (see figure 2.9); and the gaussmeter indicated the maximum perpendicular magnetic field of 350G to the target surface at the center and the maximum parallel magnetic field of 220G to the surface at 2.2cm from the center.



2.1.5 DC Power Supply

The DC power supply may maximally provide 300 watts energy. The figure 2.10 shows the dc power control panel.

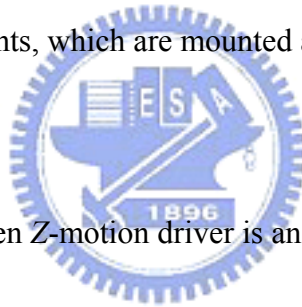
2.2 Experimental Instrumentation

2.2.1 Langmuir probe

A complete standard fixed-probe system comprises an ESPION Probe Unit

(EPIU), a gas-cooled Radio-Frequency (RF) compensated electrostatic plasma probe and all the required interconnection cabling, see Figure 2.11.

The RF-compensated electrostatic plasma probe for fixed installations and motorized Z-motion driver is shown in Figure 2.12. The tip can provide the potential ramp start from -200V to 100V and resolution 0.025V minimum. This probe is suitable for use with both DC and RF plasma; the maximum allowable temperature at the probe tip is 250⁰C, the maximum allowable temperature at the mounting flange is 70⁰C. For high temperature plasma, cooling gas may be used to limit the temperature of the compensation components, which are mounted as close to the probe as possible.



An automatic motor-driven Z-motion driver is available as an option for the probe system; see Figure 2.13.

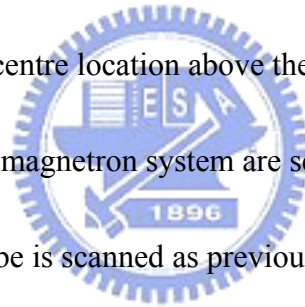
A computer-controlled stepped motor, with maximum movement of 300mm, powers the automatic Z-motion driver. The stepped motor is controlled by the PC via the EPIU and the Linear Motion Driver. A lead screw drives the probe into the chamber; vacuum sealing is provided by the flexible bellows unit.

2.2.2 Thermocouple

We could move the tip of thermocouple (see figure 2.14) to measure the temperature in the chamber or close to the substrate.

2.3 Experiment Methods and Steps

This research focuses on a spatial Langmuir probe survey of sputtering deposition plasma and the response of this plasma to process condition. The DC magnetron sputtering system employed in this investigation is depicted in figure 2.15. The research is divided into with and without magnetron system conditions. Pressures in the condition without magnetron system are set at 70 and 80 mTorr in the 99.99% argon gas and the probe is scanned horizontally across the plasma at two different cross-section in the constant distance between target and substrate and is also scanned in the normal direction at the centre location above the target. Additionally, the pressure in the condition with magnetron system are set at 10, 20 and 30 mTorr in the 99.99% argon gas and the probe is scanned as previous condition.



Chapter 3 Langmuir Probe Diagnostics

A metal probe is one of the earliest and still the most useful tools for diagnosing plasma. They are often used as plasma diagnostics because of their apparent simplicity and they are constructed easily. They measure the electron current which depends on their bias voltage with respect to the plasma potential. Over a very range of situation, the details of the $I-V$ curve characteristics can be related to the plasma parameters. These probes, introduced by Langmuir and analyzed in considerable by Mott-Smith and Langmuir are usually called Langmuir probes.

3.1 Typical $I-V$



As the probe voltage is swept with respect to the plasma potential, electrons and ions are either attracted or repelled and the net current collected by the probe changes. From the interpretation of the $I-V$ characteristic the electron distribution function, electron temperature and plasma density can be obtained. A typical voltage-current curve, in general, can be divided into three regions and two meaningful potential value points [Chen, 1965; Schott, 1955; Hershkowitz, 1989; Chung *et al.*, 1975]: 1. $V_B < V_f$: Ion saturation region. 2. $V_f < V_B < V_p$: Transition region. 3. $V_B > V_p$: Electron saturation region. 4. $V_B = V_f$: The floating potential. 5. $V_B = V_p$: The plasma potential. Generally, the current that the probe collects is the summation the electron current and

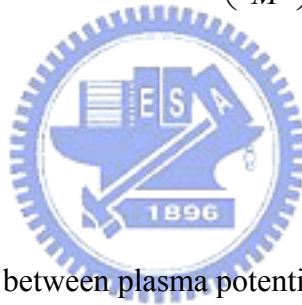
ion current and the magnitude of the ion saturation current is much smaller than the electron current due to the much greater ion saturation mass.

1. Ion saturation region:

For the potential of probe is lower than floating potential $V_B < V_f$, the current is increasingly ion current tending to an ion saturation current and almost electrons are repelled. It's not all ions can be collected by the probe. According to Bohm criterion, the velocity of ion should be accelerated over the Bohm velocity [Chen, 1965; Bohm,

1949; Lieberman and Lichtenberg, 1994] ($u_B = \left(\frac{KT_e}{M}\right)^{1/2}$) so that the ion can be

collected by the probe.



2. Transition region:

For the probe potential is between plasma potential (V_p) and floating potential (V_f), electrons are repelled according to the Boltzmann relation until at floating potential.

3. Electron saturation region:

For increasing V_B above the plasma potential, the current tends to saturate at the electron saturation current. The probe potential is positive relative to the plasma potential, electrons will be attracted and ions will be repelled. The electron sheath form in the probe surface and the electron current is limited by the thermal motion of electrons arriving to the sheath. The thickness of the sheath would increase with the

raising potential in non-planar probe. The electron saturation current is always not a constant and increase with the raising probe potential.

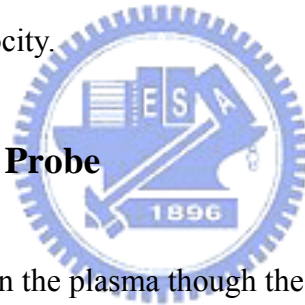
4. Floating potential:

The potential that the electron and ion currents cancel out and no net current flow through the probe is called floating potential.

5. Plasma potential:

At the probe voltage $V_B = V_p$, the probe is the same potential as the plasma and draws mainly current flowing from the more mobile electron because of the electron velocity is larger than ion velocity.

3.2 Theory of Langmuir Probe



The probe is immersing in the plasma though the structure is simple in Langmuir probe. Its theory is quite complicated. In order to simplify the probe theory, we need to do some assumptions in process of analyzing.

1. The plasma should be uniform and quasi-neutral in the condition without probe.
2. Electrons and ions must obey Maxwellian velocity distribution.
3. Electron temperature is far larger than ion temperature.
4. The mean free path of electron and ion is far larger than any characteristic length. This means there is not collision near the probe.

5. Each charged particle hitting the surface of probe will be neutralized completely and secondary electrons will not occur.

3.2.1 Planar Probe with Collisionless Sheath

Considering a flat plate probe with the physical probe area $A \gg s^2$, where s is the sheath thickness, such that the collecting area A is essentially independent of s .

A. Electron Current:

In thermal equilibrium and without perturbation in the plasma, the particle current density is

$$J_r = \frac{I}{4} N \bar{v} \quad (3.1)$$

where J_r is particle current density, N is particle number density, and $\bar{v} = \left[\frac{8KT}{\pi M} \right]^{1/2}$ is mean speed in thermal equilibrium.

Then the electron current I_e that the probe collects can be state as

$$I_e = \frac{I}{4} e N_e A \bar{V}_e \quad (3.2)$$

When $V_B \geq V_p$, all electrons move into the sheath with thermal motion. The property of plasma at the sheath edge is quasi-neutral, *i.e.*

$$N_{e\infty} \approx N_{i\infty} \equiv N_\infty$$

where $N_{e\infty}$, $N_{i\infty}$, N_∞ represent the density of electrons, ion and plasma with infinity

distance from the probe in the plasma. The saturation of electron current $I_{e,sat}$ state as:

$$I_{e,sat} = \frac{I}{4} e N_{e\infty} \overline{AV}_e = \frac{I}{4} e N_{e\infty} \overline{AV}_e \quad (3.3)$$

When $V_B < V_p$, electrons are repelled by the probe. From the previous assumption, electrons must obey Maxwellian velocity distribution function,

$$f(v_e) = N_{e\infty} \left[\frac{2KT_e}{\pi m} \right]^{1/2} \exp \left[-\frac{mv_e^2}{2KT_e} \right].$$

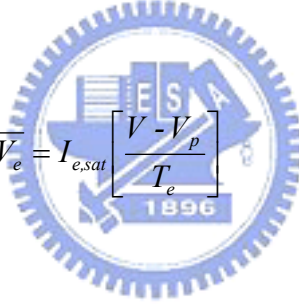
From Boltzmann relation, the electron density

becomes

$$N_e = N_{e\infty} \exp \left[\frac{V - V_p}{T_e} \right] \quad (3.4)$$

The electron current in the transition region and the ion saturation can be represents as

$$I_e = \frac{I}{4} e N_{e\infty} \exp \left[\frac{V - V_p}{T_e} \right] \overline{AV}_e = I_{e,sat} \exp \left[\frac{V - V_p}{T_e} \right] \quad (3.5)$$



B. Ion Current:

When $V_B < V_p$, ions are attracted by the probe. Because ion temperature is low, ion mass is large, the mean velocity of ion is far smaller than electrons in thermal equilibrium. It's more complicated than electrons in current analyzing.

The ion sheath will occur in the probe surface when the probe potential is lower than plasma. The electron density would then decay to shield the electrons from the wall. We will show that a transition layer or presheath must exist between the neutral plasma and nonneutral sheath in order to maintain the continuity of ion flux, giving

rise to an ion velocity at the plasma-sheath edge.

We define the zero of the potential V at $x = 0$ and the ions have a velocity u_s

there.

Ion energy conservation (in collisionless) then gives

$$\frac{1}{2}Mu^2(x) = \frac{1}{2}Mu_s^2 - eV(x) \quad (3.6)$$

The continuity of ion flux (no ionization in the sheath) is

$$n_i(x)u(x) = n_{is}u_s \quad (3.7)$$

where n_{is} is the ion density at the sheath edge. Solving for $u(x)$ from equation (3.6)

and substituting in equation (3.7) we have

$$n_i(x) = n_{is} \left(1 - \frac{2eV}{Mu_s^2} \right)^{-1/2} \quad (3.8)$$

The electron density is given by the Boltzmann relation can be stated as

$$n_e(x) = n_{es} e^{V(x)/T_e} \quad (3.9)$$

Setting $N_{es} = N_{is} \equiv N_s$ at the sheath edge and substituting N_i and N_e into

Poisson's equation

$$\frac{d^2V}{dx^2} = \frac{e}{\epsilon_0} [n_e(x) - n_i(x)] \quad (3.10)$$

We obtain

$$\frac{d^2V}{dx^2} = \frac{en_s}{\epsilon_0} \left[e^{V(x)/T_e} - \left(1 - \frac{2eV}{Mu_s^2} \right)^{-1/2} \right] \quad (3.11)$$

Multiplying above equation by dV/dx and integrating over x :

$$\int_0^V \frac{dV}{dx} \frac{d}{dx} \left(\frac{dV}{dx} \right) dx = \frac{en_s}{\epsilon_0} \int_0^V \frac{dV}{dx} \left[e^{V(x)/T_e} - \left(1 - \frac{2eV}{Mu_s^2} \right)^{-1/2} \right] dx \quad (3.12)$$

$$\frac{1}{2} \left(\frac{dV}{dx} \right)^2 = \frac{en_s}{\epsilon_0} \left[T_e e^{V(x)/T_e} - T_e + \frac{Mu_s^2}{e} \left(1 - \frac{2eV}{Mu_s^2} \right)^{-1/2} - \frac{Mu_s^2}{e} \right] \quad (3.13)$$

It is apparent that the *RHS* of the equation (3.13) should be positive. We expect this to be the problem only for small V ; we expand the *RHS* of equation (3.13) to second order in a Taylor series to obtain

$$\frac{1}{2} \frac{V^2}{T_e} - \frac{1}{2} \frac{eV^2}{Mu_s^2} \geq 0 \quad (3.14)$$

We see that

$$u_s \geq \left(\frac{eT_e}{M} \right)^{1/2} \equiv u_B \quad (3.15)$$

This result is known as Bohm sheath criterion [Langmuir, 1961] [Bohm, 1949] [Lieberman and Lichtenberg, 1994]. There must be a finite electric field in presheath region to give the ions the directed velocity u_B .

From the Bohm sheath criterion, considering that the probe is biased sufficiently negatively to collect only ion current which was collected by the probe is

$$I_{i,sat} = en_i A u_B \quad (3.16)$$

The potential drop across the presheath, which accelerates the ions to Bohm velocity, is given by

$$\frac{1}{2} Mu_B^2 = eV_p \quad (3.17)$$

Substituting for the Bohm velocity, we find

$$V_p = \frac{T_e}{2} \quad (3.18)$$

The ratio of the density at the sheath edge to that in the plasma is found from the

Boltzmann relation

$$n_s = n_\infty e^{-V_p/T_e} \approx 0.61n_\infty \quad (3.19)$$

Then we can obtain the ion current

$$I_{i,sat} = 0.61en_\infty A \left(\frac{eT_e}{M} \right)^{1/2} \quad (3.20)$$

When ion start to be repelled ($V_B > V_p$), the ion current goes to zero rapidly and

it can be state as

$$I_i = I_{i,sat} \exp\left(\frac{e(V_p - V_B)}{KT_i} \right) \quad (3.21)$$



3.2.2 Cylinder probe with collisionless sheath [Langmuir

Mott-Smith, 1926; Laframboise, 1966; Chung et al, 1975;

Lieberman and Lichtenberg, 1994]

In the previous section, we discuss the basic probe theory by the planar probe.

The planar probe would make too much perturbation in the plasma because of its large assembling surface. In practically, we would choose the cylindrical type probe to express the property of the plasma reality.

We consider first a thin wire probe for which the sheath thickness, s , is larger than the probe radius, a . In the saturation condition, only a single species is collected. A giving incoming particle in the attractive central force of the probe has initial velocity components $-v_r$ and v_ϕ in the radial and azimuthal at the edge of the sheath $r=s$. At the probe radius $r=a$, the corresponding components are $-v'_r$ and v'_ϕ . For a collisionless sheath we require conservation of energy,

$$\frac{1}{2} m(v_r^2 + v_\phi^2) + e|V_p - V_B| = \frac{1}{2} m(v_r'^2 + v_\phi'^2) \quad (3.22)$$

and conservation of angular momentum

$$s v_\phi = a v'_\phi \quad (3.23)$$

where m is the mass of the attracted species, either electrons or ions. Then we obtain

$$v_r'^2 = v_r^2 + \left(I - \frac{s^2}{a^2} \right) v_\phi^2 + \frac{2e|V_p - V_B|}{m} \quad (3.24)$$

For ion to reach the probe, setting $v_r' = 0$

$$v_{\phi 0} = \left(\frac{v_r^2 + 2e|V_p - V_B|/m}{s^2/a^2 - I} \right)^{1/2} \quad (3.25)$$

The particle only reach the probe if $|v_\phi| \leq v_{\phi 0}$.

The saturation current collected by the probe is found by integrating the radial flux $-n_s v_r$ over the distribution function at the sheath edge, for those particles that reach the probe:

$$I = -eA_s j = -e2\pi s d \int_{-\infty}^0 v_r d v_r \int_{-v_{\phi 0}}^{v_{\phi 0}} f(v_r, v_\phi) d v_\phi \quad (3.26)$$

where f is the normalized distribution function of electrons or ions. The distribution is an isotropic Maxwellian, averaged over the third velocity coordinate, we have

$$f(v_r, v_\phi) = \frac{m}{2\pi e T_s} \exp\left[-\frac{m(v_r^2 + v_\phi^2)}{2eT_s}\right] \quad (3.27)$$

where T_s is the temperature of the collected species at the sheath edge. For large probe voltage, $|V_b - V_p| \gg T_e$, we can simplify the evaluation of (equation 3.26) by assuming that

$$\frac{a}{s} \ll 1 \quad (3.28)$$

$$v_r^2 \ll \frac{e|V_p - V_B|}{m} \quad (3.29)$$

$$v_{\phi 0}^2 \ll \frac{eT_s}{m} \quad (3.30)$$

Using equation (3.28) and (3.29) to evaluate equation (3.25), we obtain

$$v_{\phi 0} = \frac{a}{s} \left(\frac{2e|V_p - V_B|}{m} \right)^{1/2} \quad (3.31)$$

Using equation (3.27) and (3.31) in equation and condition equation (3.30), we

integral to find that

$$I = 2en_s a d \left(\frac{2e|V_p - V_B|}{m} \right)^{1/2} \quad (3.32)$$

3.3 Theory of electron energy distribution function (EEDF) [Schott, 1955; Hershkowitz, 1989; Lieberman and Lichtenberg, 1994]

For the arbitrary distribution function, the electron current to a planar probe can

be written as

$$I_e = eA \int_{-\infty}^{\infty} dv_x \int_{-\infty}^{\infty} dv_y \int_{v_{min}}^{\infty} dv_z v_z f_e(v) \quad (3.33)$$

where

$$v_{min} = \left[\frac{2e(V_p - V_B)}{m} \right]^{1/2}$$

in the retarding potential region $V_p - V_B > 0$, is the minimum velocity for an electron along z at the plasma-sheath edge to reach the probe. For an isotropic distribution we can introduce spherical polar coordinates in velocity to obtain

$$I_e = eA \int_{v_{min}}^{\infty} dv \int_0^{\theta_{min}} d\theta \int_0^{2\pi} d\phi v \cos\theta v^2 \sin\theta f_e(v) \quad (3.34)$$

Where A is the physical collecting area of the probe and $\theta_{min} = \cos^{-1} \frac{v_{min}}{v}$

The ϕ and θ are integrated, yielding

$$I_e = \pi e A \int_{v_{min}}^{\infty} dv \left(1 - \frac{v_{min}^2}{v^2} \right) v^3 f_e(v) \quad (3.35)$$

Introducing the change of variable $\varepsilon = \frac{1}{2} m v^2$, then

$$I_e = \frac{2\pi e^3}{m^2} A \int_V^{\infty} d\varepsilon \varepsilon \left\{ \left(1 - \frac{V}{\varepsilon} \right) f_e[v(\varepsilon)] \right\} \quad (3.36)$$

where $v(\varepsilon) = \left(\frac{2e\varepsilon}{m} \right)^{1/2}$. Differentiating I_e we obtain

$$\frac{dI_e}{dV} = - \frac{2\pi e^3}{m^2} A \int_V^{\infty} d\varepsilon f_e[v(\varepsilon)] \quad (3.37)$$

and a second differentiation yields

$$\frac{d^2 I_e}{dV^2} = \frac{2\pi e^3}{m^2} A f_e[v(V)] \quad (3.38)$$

It is usually to introduce the electron energy distribution function (EEDF) $g_e(\varepsilon)$ by $g_e(\varepsilon)d\varepsilon = 4\pi v^2 f_e(v)dv$.

Using the relation between ε and v , we find

$$g_e(\varepsilon) = 2\pi \left(\frac{2e}{m}\right)^{3/2} \varepsilon^{1/2} f_e[v(\varepsilon)] \quad (3.39)$$

Using this to estimate f_e from (equation 38), we obtain

$$g_e(V) = \frac{2m}{e^2 A} \left(\frac{2eV}{m}\right)^{1/2} \frac{d^2 I_e}{dV^2} \quad (3.40)$$

The electron energy probability function (EEDF) $g_p(\varepsilon) = \varepsilon^{-1/2} g_e(\varepsilon)$ is sometimes introduced. For a Maxwellian distribution,

$$g_p(\varepsilon) = \frac{2}{\sqrt{\pi}} n_e T_e^{-3/2} \exp\left(\frac{-\varepsilon}{T_e}\right) \quad (3.41)$$

Obviously, we could obtain the EEDF and EEPF curves from the second order differentiation of the electron saturation current. We also could use $g_e(\varepsilon)$ to obtain the electron density n_e , average energy and effective temperature by the followed definition

$$n_e = \int_0^\infty g_e d\varepsilon$$

$$\langle \varepsilon \rangle = \frac{1}{n_e} \int_0^\infty \varepsilon g_e d\varepsilon$$

$$T_{eff} = \frac{2}{3} \langle \varepsilon \rangle$$

3.4 Parameter Calculation

As the probe voltage is swept with respect to the plasma potential, electrons and ions are either attracted or repelled and the net current collected by the probe changes.

From the interpretation of the $I-V$ characteristic the electron distribution function, electron temperature and plasma density can be obtained.

1. Plasma potential:

From $I-V$ curve, we may obtain the plasma potential directly by $\frac{dI}{dV_B} = \max$ or $\frac{d^2I}{dV_B^2} = 0$.

2. Plasma density:

In ion saturation region, the ion saturation current can be state as

$$I = 2en_s ad \left(\frac{2e|V_p - V_B|}{m} \right)^{1/2}$$

And a plot of I^2 versus V_B should be linear, with n_s^2 by the slope of this line, independent of T_e and T_i .

3. Electron temperature:

In the transition and electron saturation region, the current can be state respectively as

$$I_e = \frac{I}{4} eN_{e\infty} \exp \left[\frac{V_B - V_p}{T_e} \right] A \bar{V}_e$$

and

$$I_{e,sat} = \frac{I}{4} e N_{e\infty} \overline{AV}_e$$

Comparing above equations and taking the logarithm, we have

$$\ln\left(\frac{I_e}{I_{e,sat}}\right) = \frac{V_B - V_P}{T_e}$$

From above equation we see that the electron temperature can be written as

$$T_e(eV) = \left(\frac{d(\ln I)}{dV_B}\right)^{-1}$$

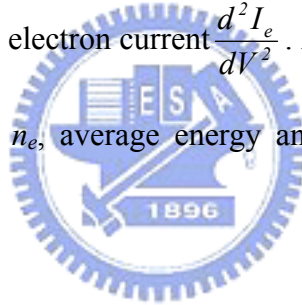
4. EEDF theory:

We can obtain the electron energy distribution function (EEDF), $g_e(\varepsilon)$, from the secondary differential of the electron current $\frac{d^2 I_e}{dV^2}$. And using $g_e(\varepsilon)$ that we could obtain the electron density n_e , average energy and effective temperature by the followed definition

$$n_e = \int_0^\infty g_e d\varepsilon$$

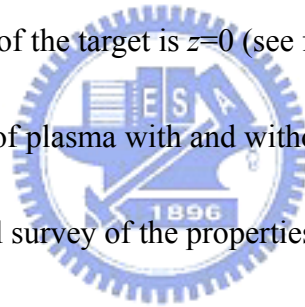
$$\langle \varepsilon \rangle = \frac{1}{n_e} \int_0^\infty \varepsilon g_e d\varepsilon$$

$$T_{eff} = \frac{2}{3} \langle \varepsilon \rangle$$



Chapter 4 Results and Discussion

We can obtain lots of properties of plasma from the $I-V$ curve measured by the electrostatics probe. The object we will measure is the DC sputtering chamber in MuST laboratory. The probe was driven by the Z -motion will pass through above the target from the left side to the right side. We started to measure the $I-V$ curve from the point 8cm besides left the center of the target to the point 8cm besides right the centre of the target and we set the center of the target is $x=0$ (see figure 4.1). We also set the distance of the horizontal cross section to the surface of the target is Z and the surface of the target is $z=0$ (see figure 4.1). We will show the $I-V$ curves and the properties of plasma with and without magnetron in this chapter. Then, we will show the spatial survey of the properties of a sputtering plasma system between the substrate and the target.



4.1 The discharges with magnetron

An aluminum target is used with 99.99% purity argon gas at pressures of 10 mtorr, 20 mtorr and 30 mtorr and the magnetron assembly was installed under the cathode. Figure 4.2 shows the picture of the discharge with magnetron assembly and we can see the extreme glowing region above the target. The target voltage for every scan was 310 V at 10 mtorr, 270 V at 20mtorr and 250 V at 30mtorr; currents at 0.4 A, 0.48 A and 0.51 A respectively. Two horizontal surveys are

completed for each pressure at distances 4 and 6 cm from the cathode in the gap distance 8 cm between the target and the substrate. Four horizontal surveys are also completed for each pressure at distances 4, 6, 8 and 10 cm from the cathode in the gap distance 11 cm between the target and the substrate.

4.1.1 Plasma potential and floating potential

The plasma potential of the horizontal surveys is presented from the figure 4.3 to the figure 4.5. There is a slight variation in plasma potential for each horizontal and vertical survey. This weak change in plasma potential indicates that there is a very weak electric field in the plasma.

The floating potential in contrast to plasma potential has a strong dependence on the pressure and the spatial position. We could see horizontal distribution of floating potential from figure 4.6 to figure 4.8 and vertical distribution in figure 4.9. We can find that in the outer edge of the cathode the floating potential is near to 0 V but drops to minus when the probe moved into the center of the cathode. In the vertical distribution, we can also find that the floating potential far away the cathode is larger than the floating potential closing to the cathode.

The floating potential is dependent on the relative flux of electrons and ions to the probe where the flux depends on the density and energy of the respective species. Because of the plasma is quasineutral, any inconsistency in flux will result

the energy differences between the electron and positive ions. Due to the great difference in mass, the electrons are more mobile than the ions so the floating potential is expected to depend on the electron energy. Hence, the changes in the floating potential should be mirrored by changes to the electron energy or the electron temperature.

From the concept of floating potential, we can equate the ion flux to the electron flux, i.e. $\Gamma_i = n_s u_B = \frac{I}{4} n_s \bar{v}_e e^{\Phi_w / T_e} = \Gamma_e$. Solving for Φ_w (the potential of the probe respect to the sheath-presheath edge), we obtain $\Phi_w = -T_e \ln \left(\frac{M}{2\pi m} \right)^{1/2}$.

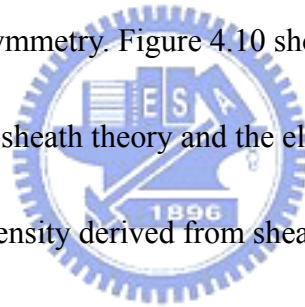
For argon gas, we can calculate $\Phi_w = -4.7T_e$. This means the argon ion with initial energy $\varepsilon_s = 0.5T_e$ fall through a collisionless dc sheath to a floating probe with energy of $\varepsilon_i \approx 5.2T_e$. We could preliminary estimate the value of $\frac{V_p - V_f}{T_e}$ would be around 5.2 ideally. Table 1~3 show the value of $\frac{V_p - V_f}{T_e}$ in different places in the chamber. The values are a little less than the ideal value. This means we could overestimate the electron temperature or underestimate the plasma potential.

4.1.2 Plasma density

In the previous chapter, we talk about the sheath theory and electron energy distribution function (EEDF). These two kinds of theories have different functions and the properties can be analyzed are different. We can obtain electron temperature,

plasma density and plasma potential via sheath theory. In the other hand, we could obtain electron temperature and plasma density via electron energy distribution function (EEDF) theory.

For the sheath theory, *i.e.* OML theory, we could obtain the plasma density and it also required a thick sheath. On the other hand, the electron energy distribution function is not affected by the thickness of the sheath and it also doesn't require the distribution of the electron energy obey the Maxwellian distribution. The theory of electron energy distribution function is derived from the planar probe so it couldn't show the completely spatial symmetry. Figure 4.10 shows the differences of plasma density between derived from sheath theory and the electron energy distribution function theory. The plasma density derived from sheath theory is a little larger than the plasma density from EEDF in the same position.



We also show the horizontal survey in the figure 4.11 and 4.12, and in these figures the plasma density has larger value in the center of the target. In the outer field of the cathode have lower value of the plasma density. In figure 4.13 with the probe which was located above the center of the cathode, it shows the plasma density decrease with the probe move up away the cathode. It makes sense that this location close to the cathode (inside the magnetic trap) would record the highest electron density and that at greater distances vertical to the cathode the density would fall as

plasma diffuses outwards.

4.1.3 Electron temperature

There are two ways to obtain the electron temperature as we have remarked before. We could obtain the electron temperature from the analysis of the curve of the electron current but the electron energy distribution should be obeyed the Maxwellian distribution first. Fortunately, most of the data are closing to the Maxwellian distribution and we could receive the meaningful electron temperature.

In the theory of electron energy distribution function, it is using the method of the averaged energy of distribution function as following equations. The equation 4.2 uses T_{eff} to represent the effective electron temperature. The advantage of EEDF is that the results are not influenced by the electron energy distribution and response the instantaneous state of the plasma. We could find the difference of the electron temperature derived from sheath theory and EEDF in the figure 4.16.

$$\langle \varepsilon \rangle = \frac{I}{n_e} \int_0^{\infty} \varepsilon g_e d\varepsilon \quad (4.1)$$

$$T_{eff} = \frac{2}{3} \langle \varepsilon \rangle \quad (4.2)$$

As the previous mentioned, the electron temperature is mirrored to the change of the floating potential. In the figure 4.14 and 4.15, it shows the horizontal distribution of electron temperature above the cathode. At the outer edges of the cathode the electron temperature, T_e , is under 0.5 eV but rapidly rise to over 1 eV even closing to

2 eV above the center of the cathode. In figure 4.17 with the probe located above the center of the cathode, it shows the electron temperature decrease with the probe move up away the cathode. It makes sense that the plasma power source closes to the cathode would generate the highest electron temperature and that at greater distances vertical to the cathode the electron temperature would fall as more collisions occurred outwards. We also can find the trend that the higher working pressure could lead to lower electron temperature in figure 4.18. It could be realized that the more gas molecules mean the more collisions occur and the electrons would lose its energy after every collision.

4.2 The discharges without magnetron

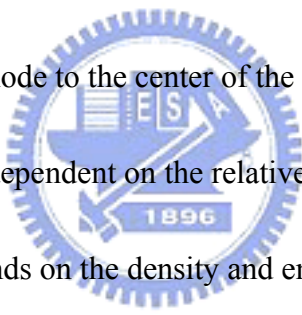


In the discharges condition without magnetron, we also used an aluminum target and 99.99% purity argon gas at pressures of 70 mtorr and 80 mtorr and removed the magnetron assembly under the cathode. Figure 4.19 shows the picture of the discharge without magnetron. According to the Paschen curve, we need the higher applied voltage to make the gas discharge. The target voltage for every horizontal scan was 710 V at 70 mtorr and 700 V at 80 mtorr; currents at 0.01 A. Two horizontal surveys are completed for each pressure at distances 2 and 3 cm from the cathode in the gap distance 4 and 5 cm between the target and the substrate.

4.2.1 Plasma potential and floating potential

The plasma potential of the horizontal surveys is presented from the figure 4.20. The variation in plasma potential is larger than the condition with magnetron for each horizontal survey. This small change in plasma potential indicates that there is a weak electric field in the plasma.

The floating potential in contrast to plasma potential has a strong dependence on the spatial position. We could see horizontal distribution of floating potential in figure 4.21. We can find that the floating potential decrease when the probe move from the outer edge of the cathode to the center of the cathode.



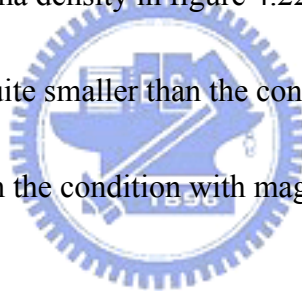
The floating potential is dependent on the relative flux of electrons and ions to the probe where the flux depends on the density and energy of the respective species as we have mentioned before. Because of the plasma is quasineutral, any inconsistency in flux will result the energy differences between the electron and positive ions. Duo to the great difference in mass, the electrons are more mobile than the ions so the floating potential is expected to depend on the electron energy. Hence, the changes in the floating potential should be mirrored by changes to the electron energy or the electron temperature.

As mentioned concept of floating potential in the section 4.1.1, we could state a relation among V_p , V_f and T_e . From table 4 and table 5, we could find the values of

$\frac{V_p - V_f}{T_e}$ are larger than the ideal value, *i.e.* 5.2. This means the electron temperature is underestimated and plasma potential is overestimated in the condition operated without magnetron.

4.2.2 Plasma density

We could obtain electron temperature and plasma density via electron energy distribution function (EEDF) theory and sheath theory. The advantages and disadvantages of the both methods had been mentioned before. We could find the horizontal distribution of plasma density in figure 4.22. We also find out that the plasma density is obviously quite smaller than the condition with magnetron even the working pressure is larger than the condition with magnetron.



4.2.3 Electron temperature

There are two ways to obtain the electron temperature as we have remarked before. We could obtain the electron temperature from the analysis of the curve of the electron current but the electron energy distribution should be obeyed the Maxwellian distribution first. Fortunately, most of the data are closing to the Maxwellian distribution and we could receive the meaningful electron temperature by both of above methods.

As the previous mentioned, the electron temperature is mirrored to the change of

the floating potential. We also can find that the greater distances horizontal to the center of the cathode and the electron temperature would fall down from figure 4.23 even though the range of decreasing is not large. The electron temperature did not rise greatly from the outer of the cathode to the center of the cathode.



Chapter 5 Conclusions and Future Work

5.1 Summary

In the previous chapter, it could be found that we were dealing with two different conditions. One condition is the system without the magnetron and another condition is the system with the magnetron. The discharge system would need the higher pressure and the system cannot be applied larger currents when system was operated without the magnetron. The results of the distribution of plasma properties were not symmetric as our expectation at beginning in both of conditions. We make the coordinate move 4 cm right and the symmetry seems to be improved. It was found, in general, that the pressure increased could lead density increasing at the same system conditions. It also could be found that the electron temperature and the density increased and floating potential decreased when the probe moved forward into the centre of the target.

The system with magnetron can generate the greater plasma density than the system without magnetron, although the system with magnetron would be operated in the lower pressure. The density and the electron temperature decrease progressively with the distance of vertical the cathode increasing in the system with magnetron. Because of the small variation of plasma potential, the electrical field in the plasma is quite small. The changes of the floating potential could reflect the variation of the

electron temperature, *i.e.* the floating potential decrease and the electron temperature increase.

5.2 Recommendations for Future Work

This is a preliminary research to survey the special distribution of plasma characteristics and it still has a lot of problems need to overcome. We could obtain the different current values by applying a voltage bias when we install the electrostatic probe into the plasma. However, it also disturbed the environment of the plasma. To minimize the effects of the electrode that was on the probe was the following problems needed to be solved.

When we put the magnetron into the system, the system can be operated in the lower pressure. It also increased the sputtering phenomenon and it led the lots of aluminum coated on the surface of the probe. Since the aluminum is the conductive material, it seems to coat an electrode on the probe and increases the thickness of the tip. It is also important to clean the probe after the measurement and decrease the time in the measurement.

Reference

1. Boyd, R. L. F. and Twiddy, N. D., "Electron energy distributions in plasmas", Proc. Roy. Soc., A205, pp. 53-69, 1959.
2. Bohm, D., "Minimum Ionic Kinetic Energy for a Stable Sheath" in The Characteristics of Electrical Discharges in Magnetic Fields (A. Guthrie and R. K. Walkerling) McGraw-Hill Book, New York, 1949.
3. Chen, F. F., "Electric Probes." In Plasma Diagnostic Techniques (R. H. Huddleston and S. L. Leonard, eds.), Academic Press, New York, 1965.
4. Chung, P. M., Talbot, L. and Touryan, K. J., "Electric Probes in Stationary and Flowing Plasmas: Theory and Application, Springer Verlag", New York, 1975.
5. Druyvesteyn, M. J., Z. Phys., 64, pp. 781-798, 1930.
6. Druyvesteyn, M. J. and Warmoltz, N., Phil. Mag., 17, pp. 1, 1935.
7. Hershkowitz, I. H., "Principles of Plasma Diagnostics", Cambridge University Press, Cambridge, 1987.
8. Hershkowitz, Noah, "How Langmuir Probes Work" in Plasma Diagnostics vol.1 Discharge Parameters and Chemistry (Orlando Auciello and Daniel L. Flamm) Academic Press, London, 1989.
9. Heiden Analytical, ESPION User Manual.
10. Heiden Analytical, ESPsoft User Manual.

11. Johnson, E. O. and Malter, "Double-Probe Method for Determination of Electron Temperatures in Steady and Time-Varying Gas Discharges", *L., Phys. Rev*, 76, pp. 1411, 1949.
12. Johnson, E. O. and Malter, "A Floating Double Probe Method for Measurements in Gas Discharges", *L., Phys. Rev*, 80, pp. 58, 1950.
13. Laframboise, J. G., "Institute for Aerospace Studies Report No. 100", University of Toronto, 1966.
14. Langmuir, I. and Mott-Smith, H. M., *Gen. Elec. Rev.*, 26, pp. 731, 1923; 27, pp. 449, 583, 616, 726, 810, 1924.
15. Langmuir, I. and Mott-Smith, H. M., "The Theory of Collectors in Gaseous Discharges", *Phys. Rev.*, 28, pp. 727-763, 1926.
16. Langmuir, I., "The Collected Worked of Irving Langmuir, ed. G. Suits", Pergamon Press, Inc., New York, 1961.
17. Lieberman, M. A. and Lichtenberg A. J., "Principles of Plasma Discharges and Material Processing", A Wiley-Interscience Publication, New York, 1994.
18. Okuda, T. and Yamamoto, K, J. "Asymmetrical Triple Probe Method for Determining Energy Distribution of Electron in Plasma", *Appl. Phys.*, 31, pp. 158-162, 1960.
19. Raizer, Y. P., "Gas Discharge Physics", Springer-Verlag, 1991.

20. Rossnagel, S. M. and Kaufman, H. R., "Langmuir probe characterization of magnetron operation" J. Vac. Sci. Technol., A 4, pp. 3, May/Jun, 1986.
21. Schneider, W. H., Acta. Phys. Austriaca, 10, pp. 54, 1956.
22. Schott, L, "Electrical Probes," in Plasma Diagnostics (W. Lochte-Holtzgreven), AIP Press, New York, 1995.
23. Seo, S-H, In, J-H, and Chang, H-Y, "Effect of duty cycle on plasma parameters in the pulsed dc magnetron argon discharge" Appl. Phys. Lett., 86, 262103, 2005.
24. Swift, J. D. and M. J. R., "Electric Probes for Plasma Diagnostics", Iliffe Books, London, 1971.
25. Qin, S. and Mcteer A., "Time-delayed, time-resolved Langmuir probe diagnostics of pulsed plasmas" Appl. Phys. Lett., 87, 241506, 2005.
26. Wu, S. Z., "Dependence of plasma characteristics on dc magnetron sputter parameters" J. Appl. Phys., 98, 083301, 2005.
27. Yamamoto, K. and Okuda, T., "On the Floating Probe Method for the Measurement of Ionized Gas", J. Phys. Soc. Japan, 11, pp.57-68, 1956.



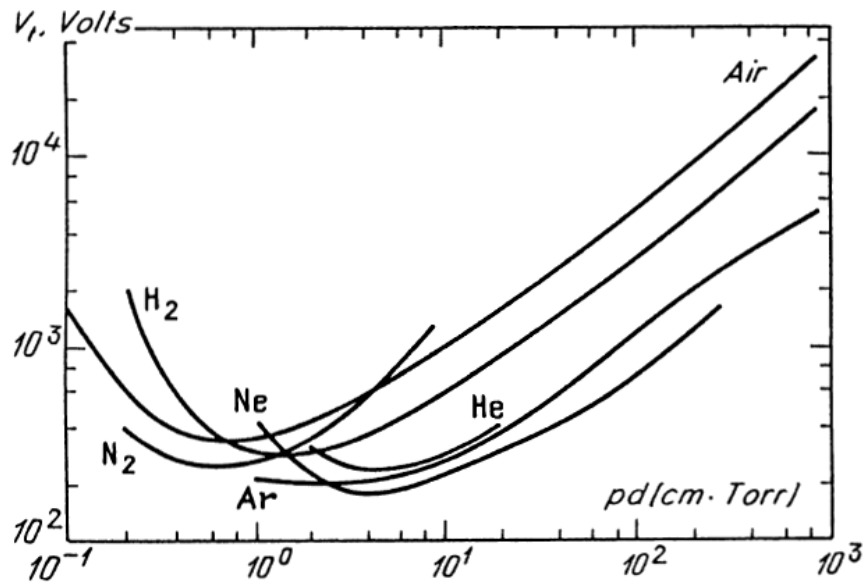


Figure 1.1. Breakdown voltages in various gases for the plane parallel

electrode [Raizer, 1991]

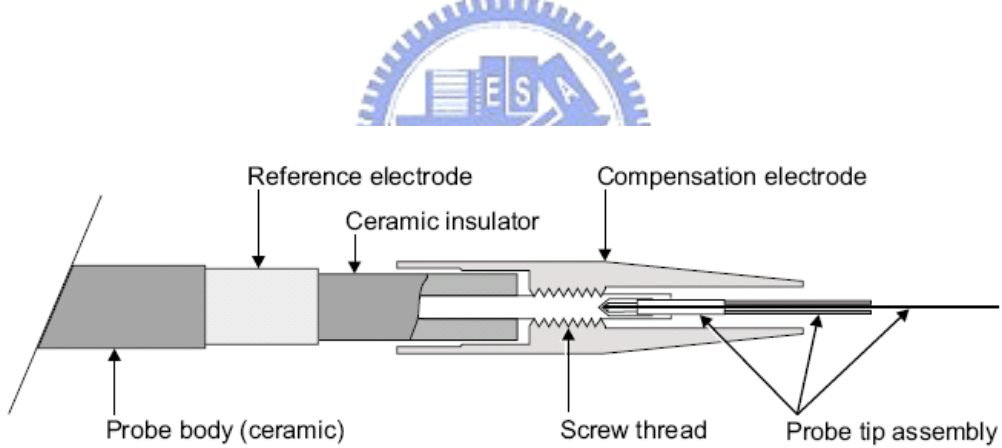


Figure 1.2. Construction of a cylindrical probe

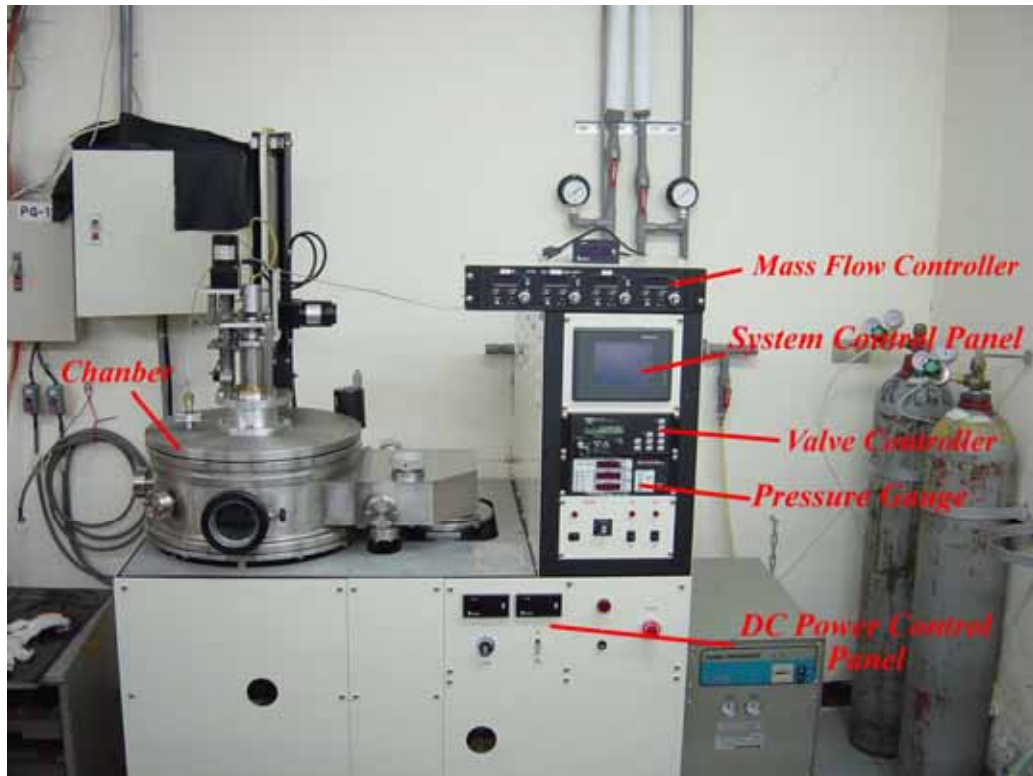


Figure 2.1. The DC-magnetron Sputtering System



Figure 2.2. The MKS self-tuning controller



Figure 2.3. The Baratron capacitance manometer



Figure 2.4. The Wide-Range Vacuum Gauge Controllers



Figure 2.5. The ion gauge



Figure 2.6. The thermocouple gauge

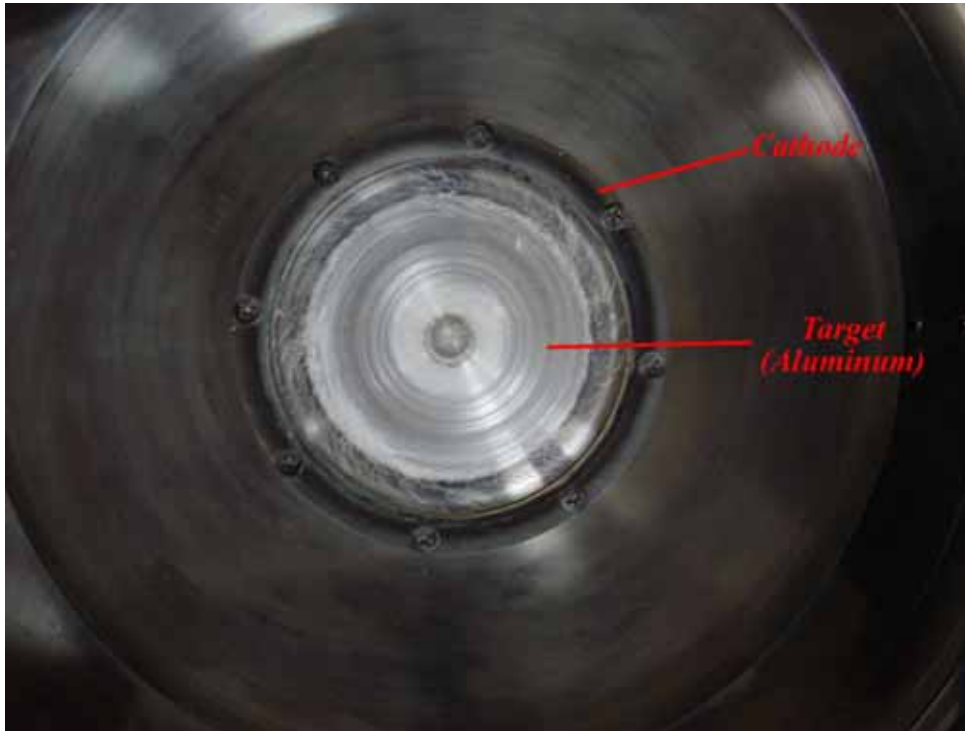


Figure 2.7. The plasma source

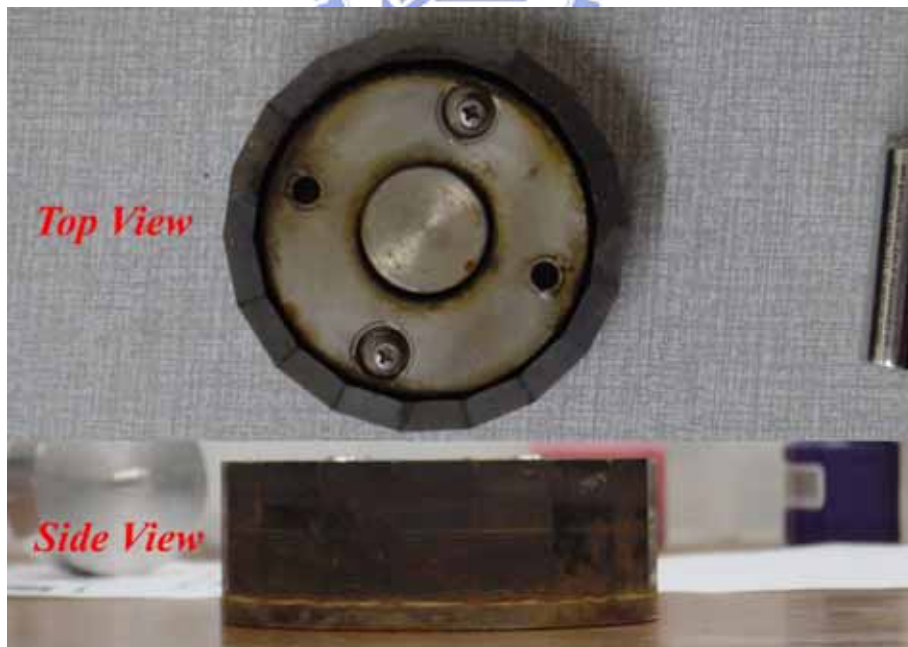


Figure 2.8. The Magnetron System



Figure 2.9. The LakeShore 421 Gaussmeter



Figure 2.10. The DC power control panel

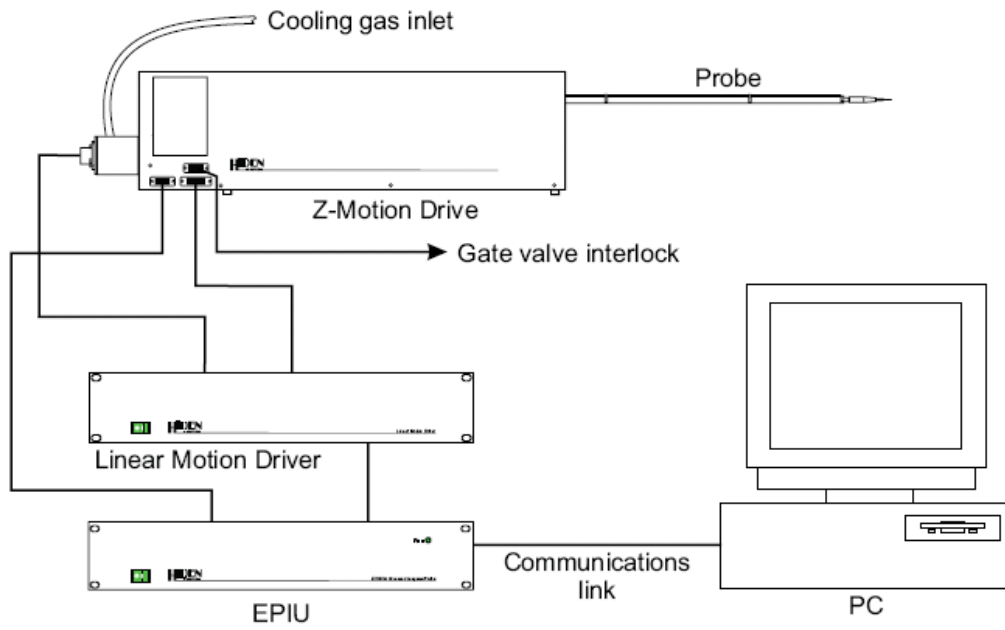


Figure 2.11. Standard ESP analysis system with motorized Z-motion control

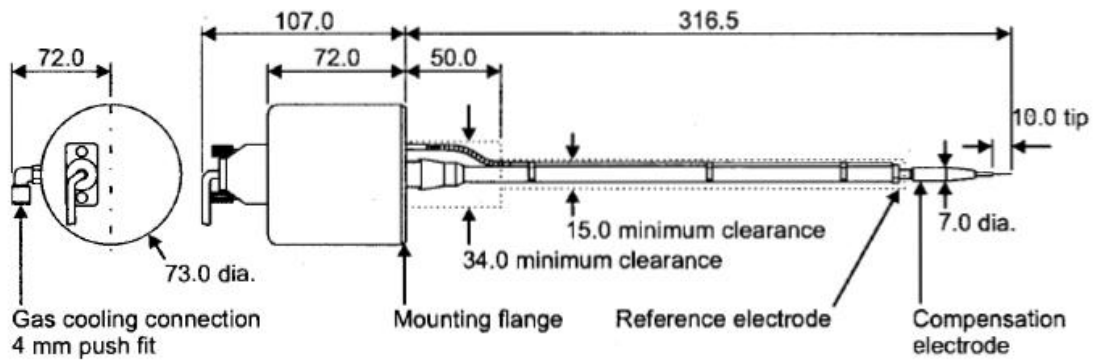


Figure 2.12. RF-compensated probe

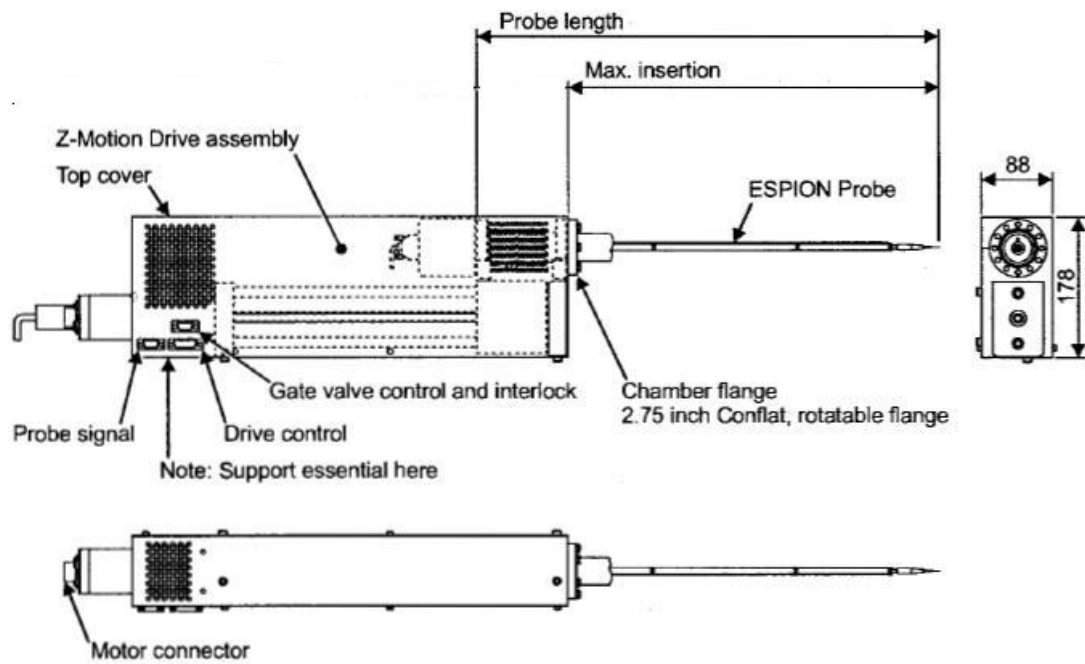


Figure 2.13. Automatic Z-motion drivers



Figure 2.14. The position of thermocouple in the chamber

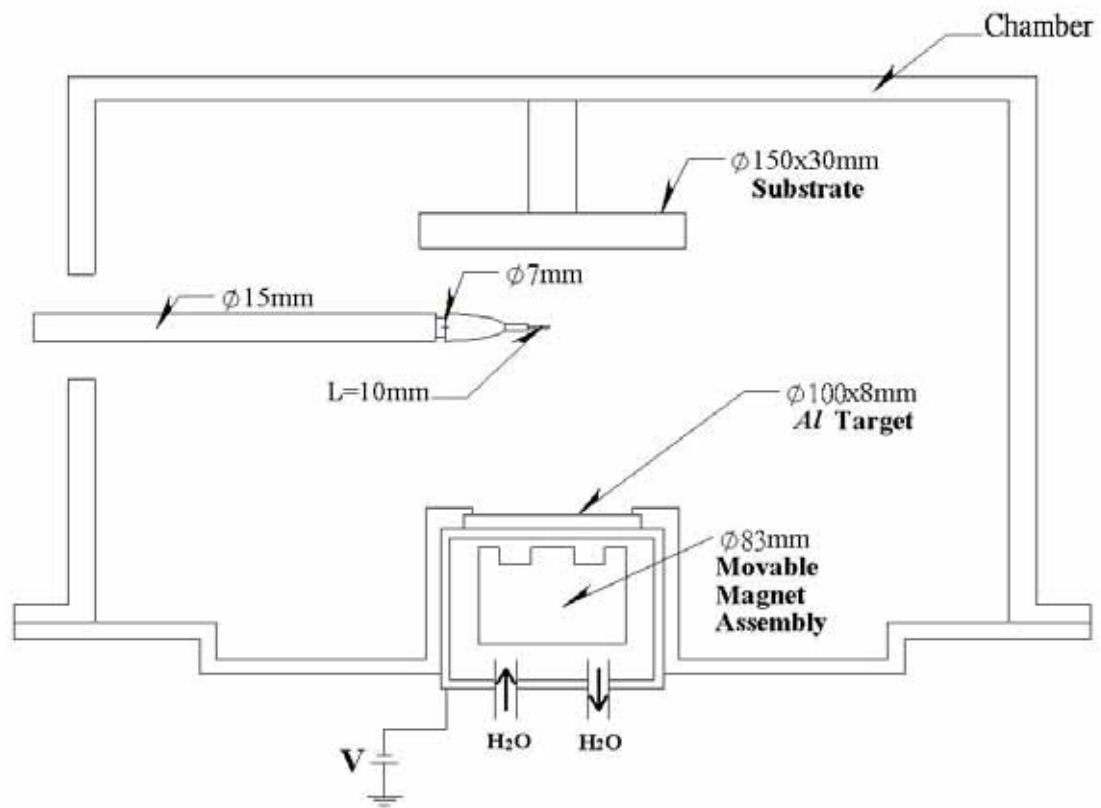


Figure 2.15. Schematic of experimental chamber

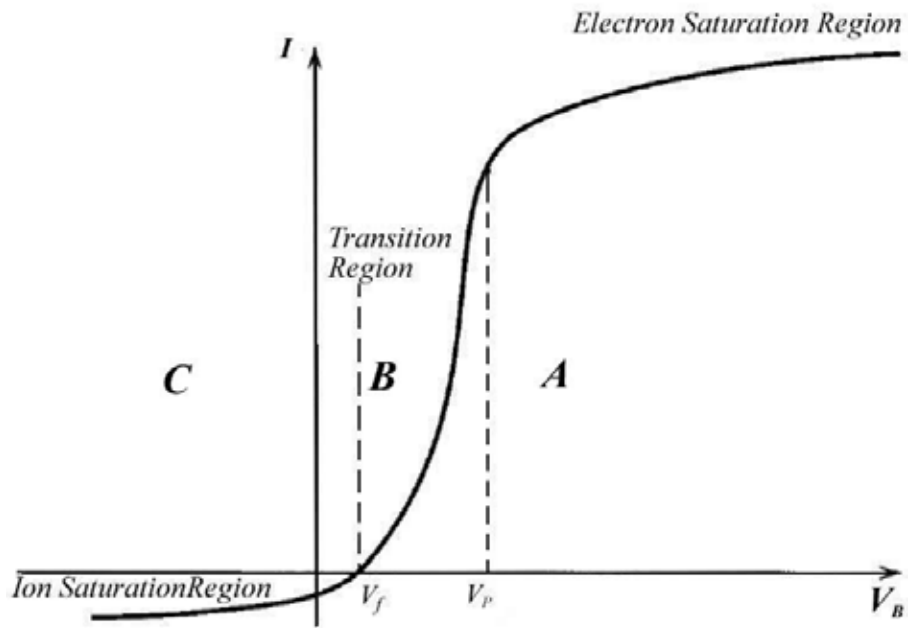


Figure 3.1. Typical I - V curves for Langmuir probe

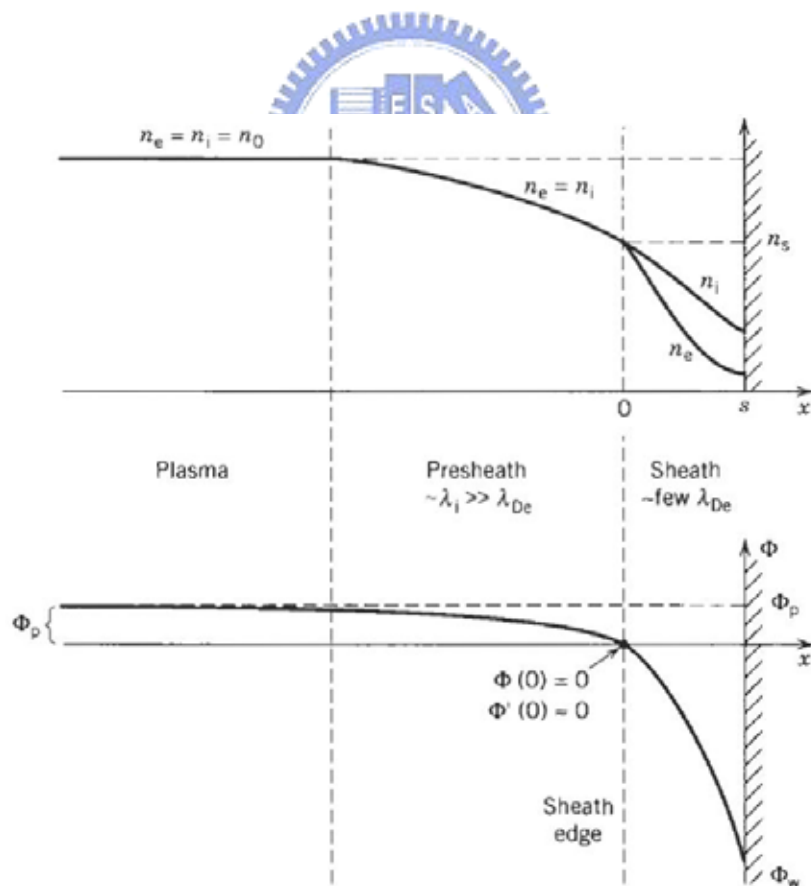


Figure 3.2. Qualitative behavior of the sheath and presheath in contact with a wall [Lieberman and Lichtenberg, 1994]

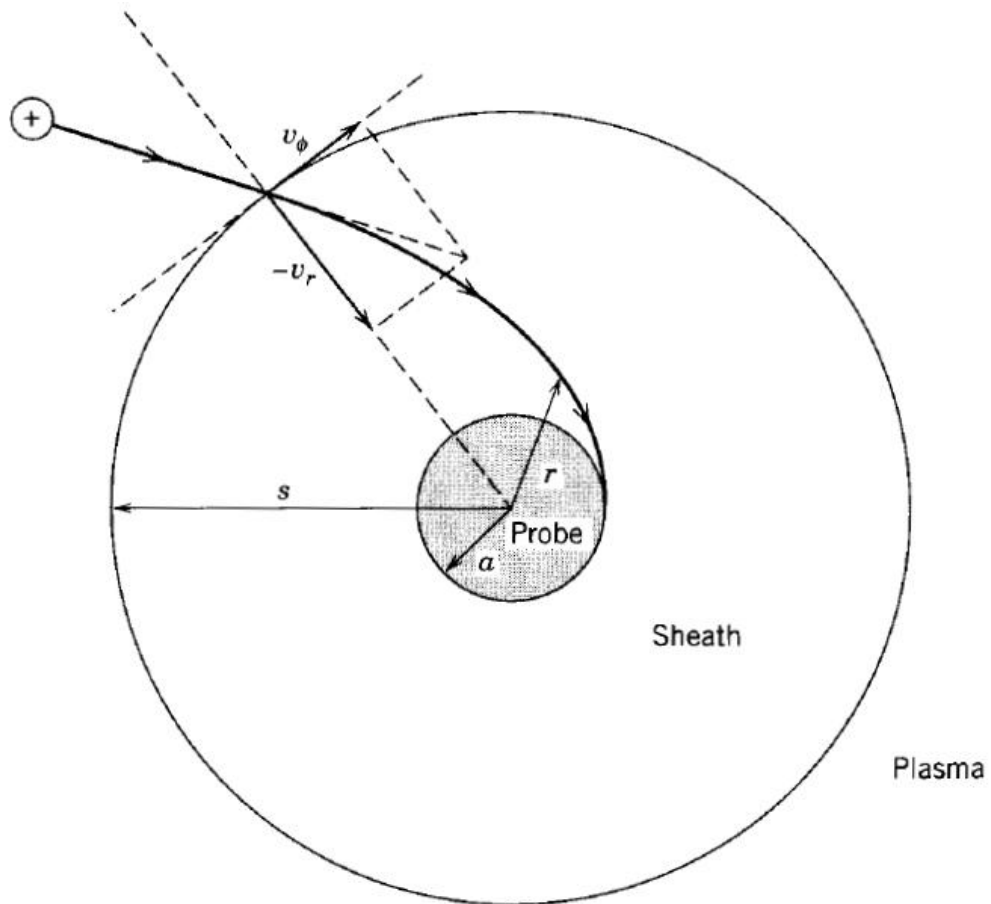
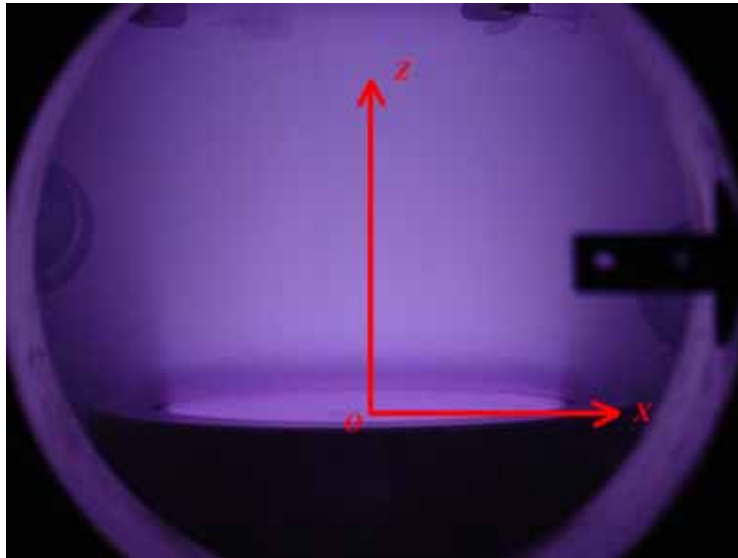
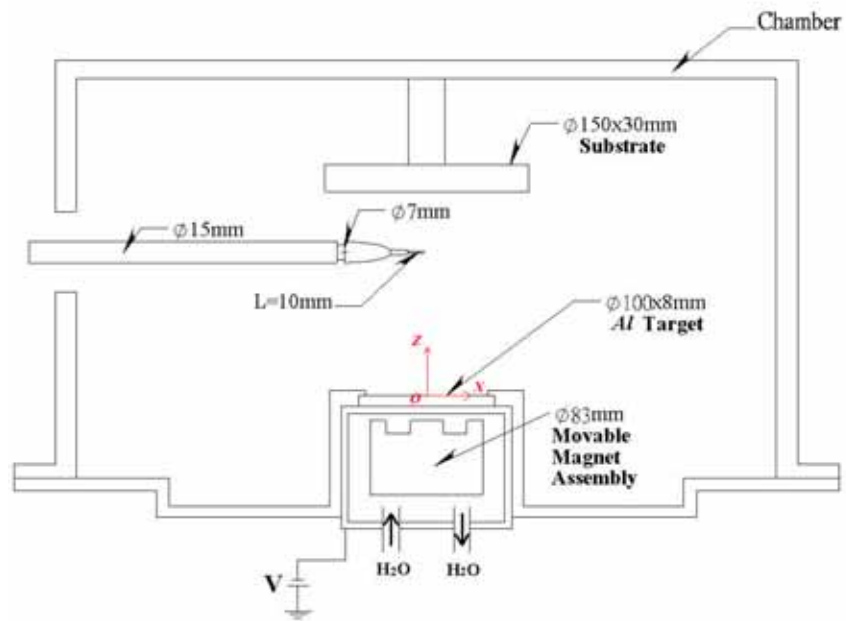


Figure 3.3. Ion orbital motion within the sheath of a cylindrical Langmuir probe [Lieberman and Lichtenberg, 1994]



(a)



(b)

Figure 4.1. The coordinate in the chamber where the origin is on the center of the target surface. (a) the coordinate is on the picture (b) the coordinate is on the schematic of experimental chamber

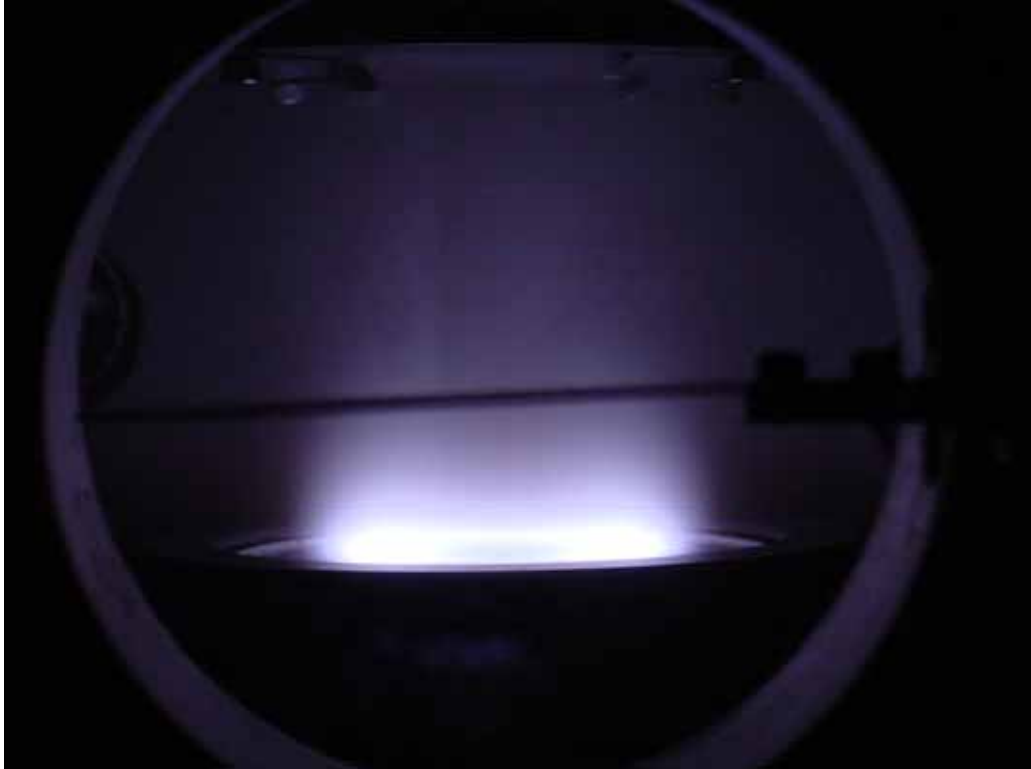
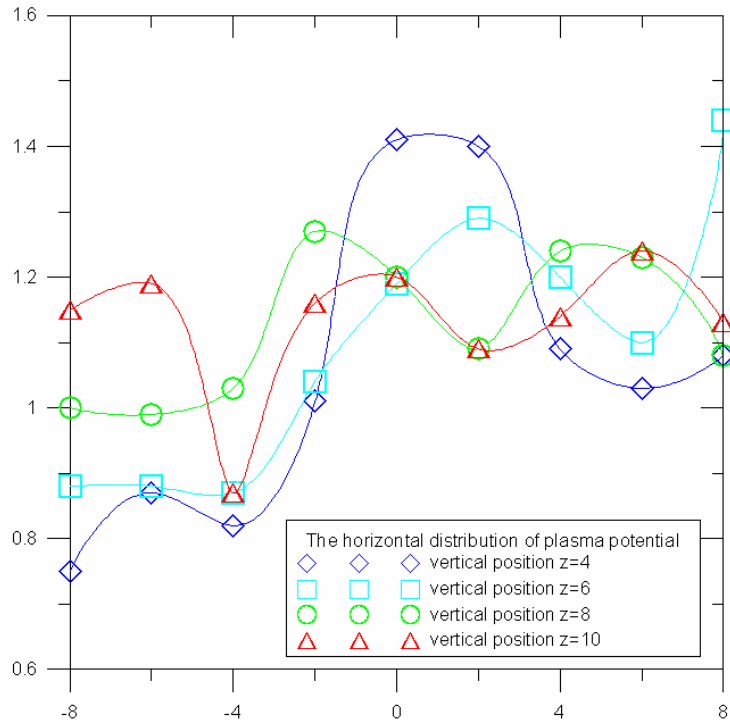
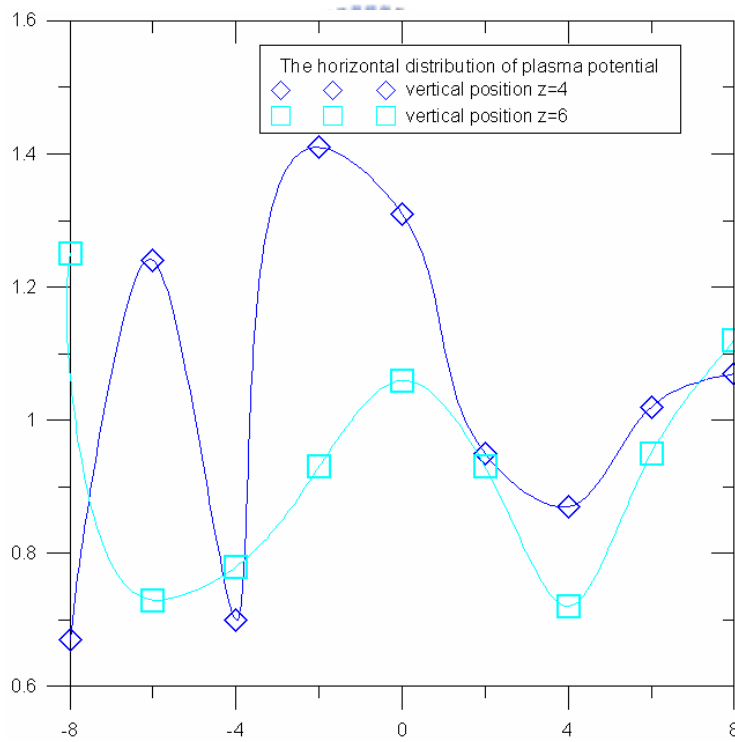


Figure 4.2. The discharge was operated with the magnetron assembly in the pressure 10 mtorr



(a)



(b)

Figure 4.3. The horizontal distribution of plasma potential in the pressure 30 mtorr and the distance between substrate and target is (a) 11 cm and (b) 8 cm.

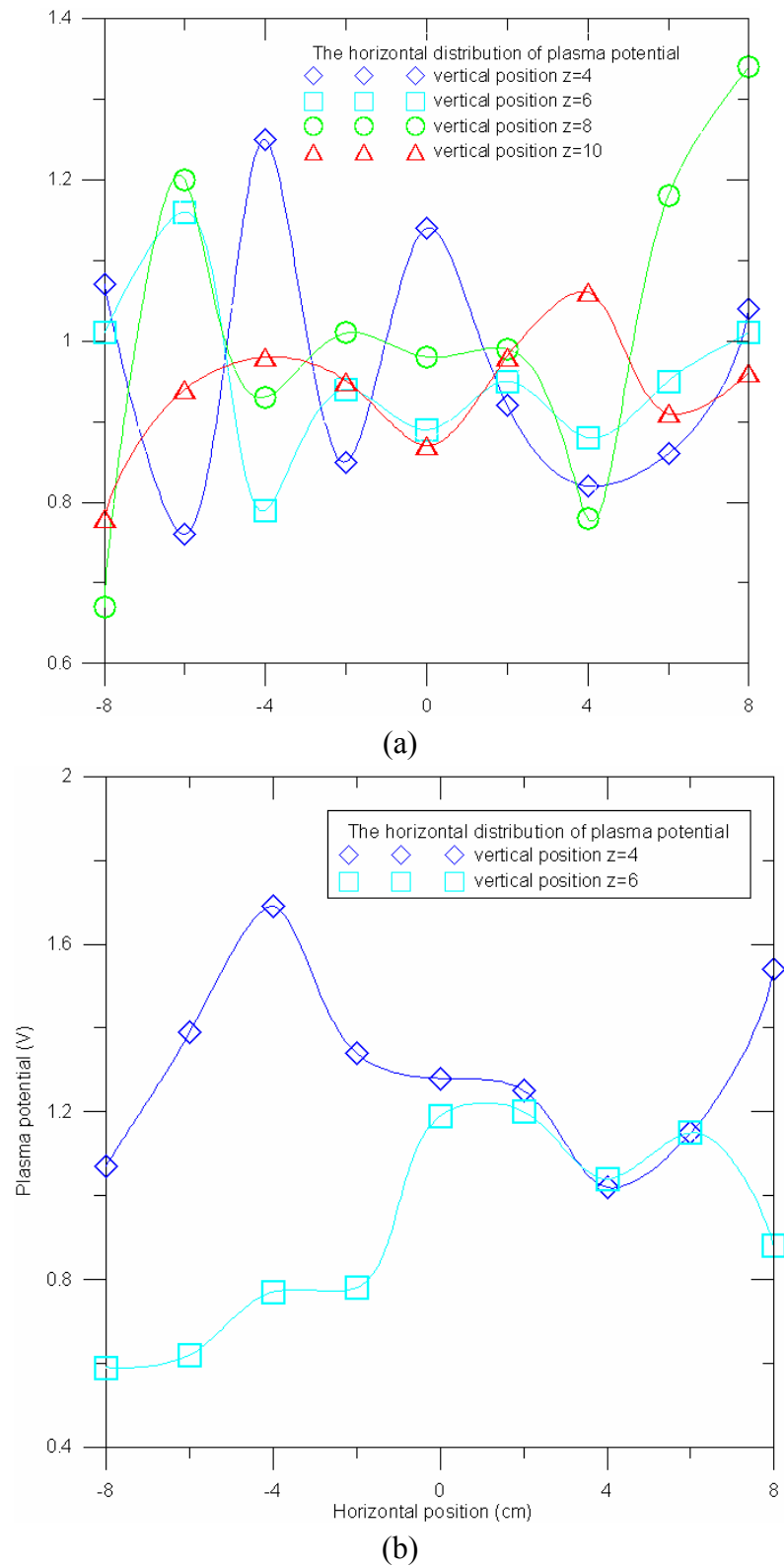
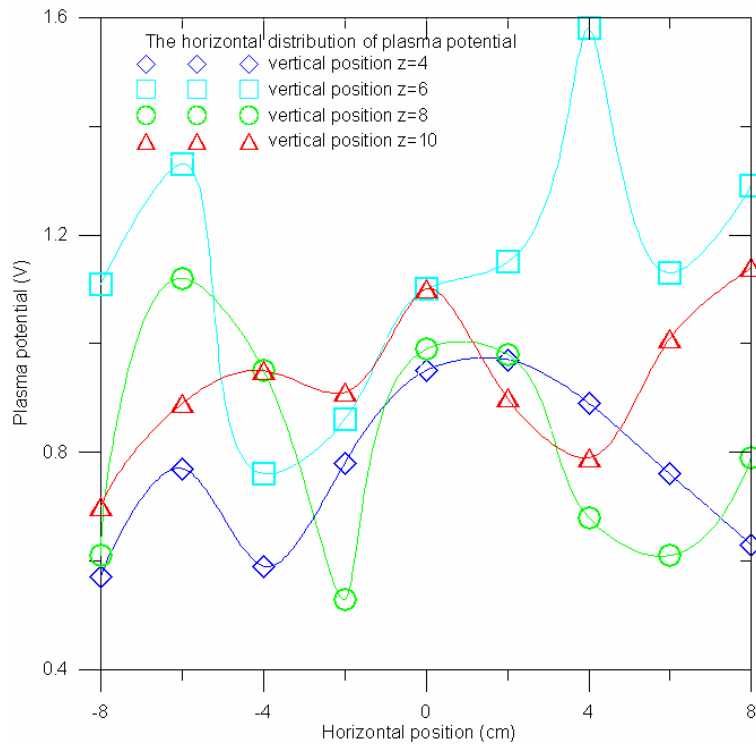
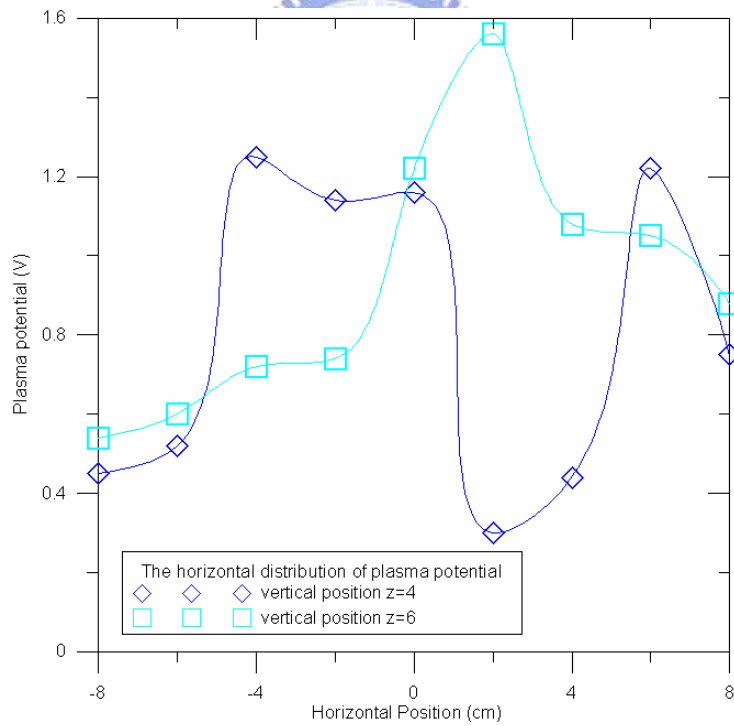


Figure 4.4. The horizontal distribution of plasma potential in the pressure 20 mtorr and the distance between substrate and target is (a) 11 cm and (b) 8 cm.

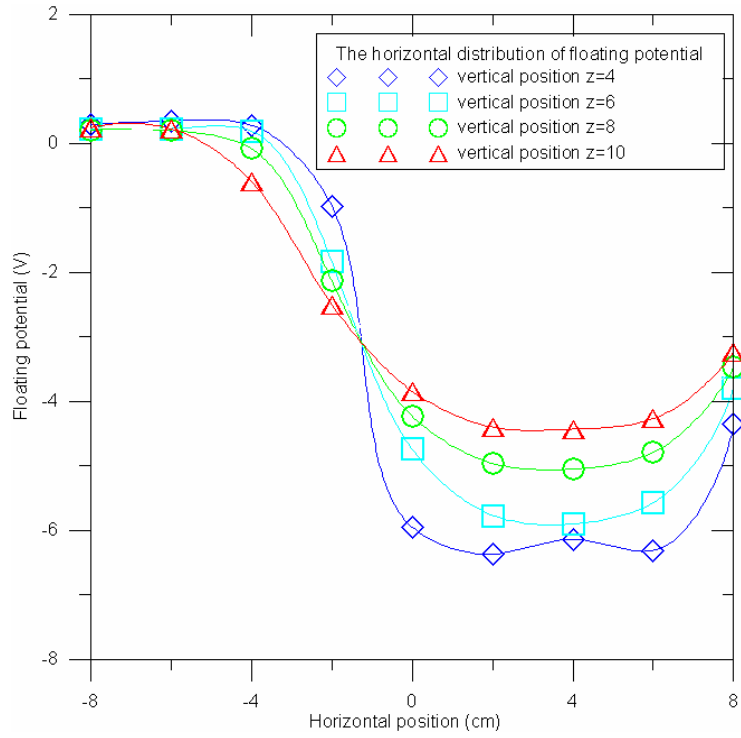


(a)

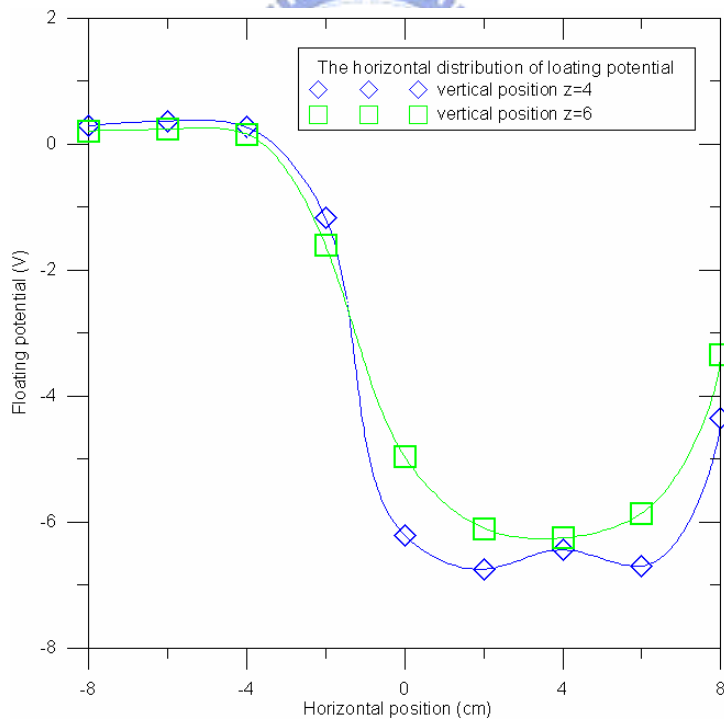


(b)

Figure 4.5. The horizontal distribution of plasma potential in the pressure 10 mtorr and the distance between substrate and target is (a) 11 cm and (b) 8 cm.

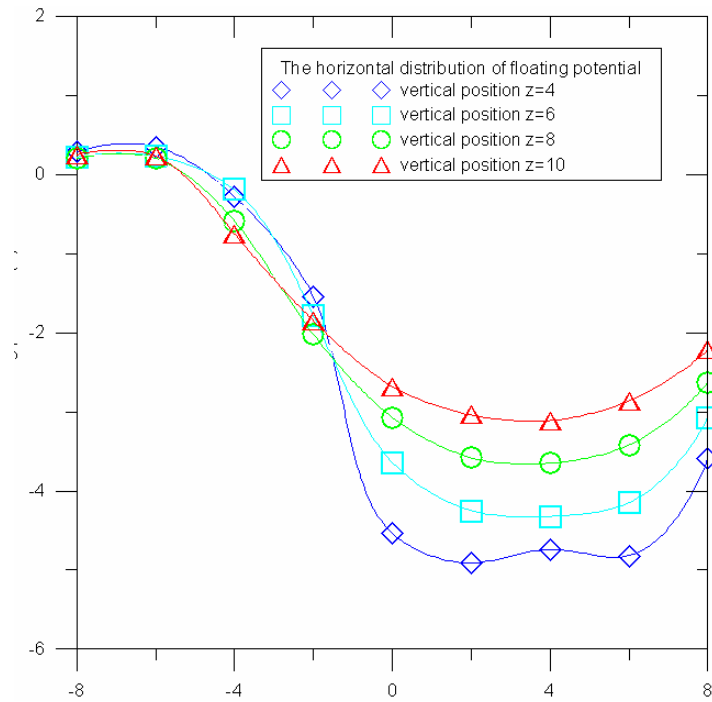


(a)

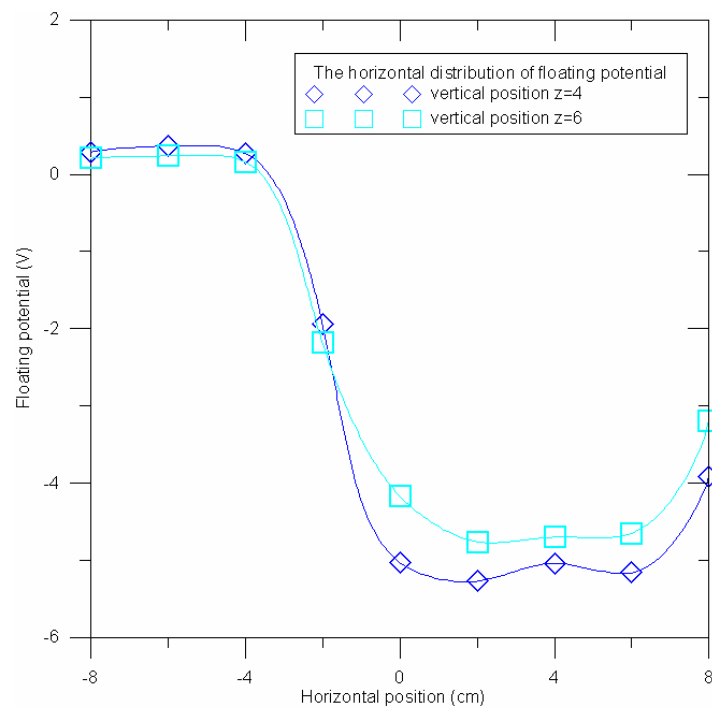


(b)

Figure 4.6. The horizontal distribution of floating potential in the pressure 10 mtorr and the distance between substrate and target is (a) 11 cm and (b) 8 cm.



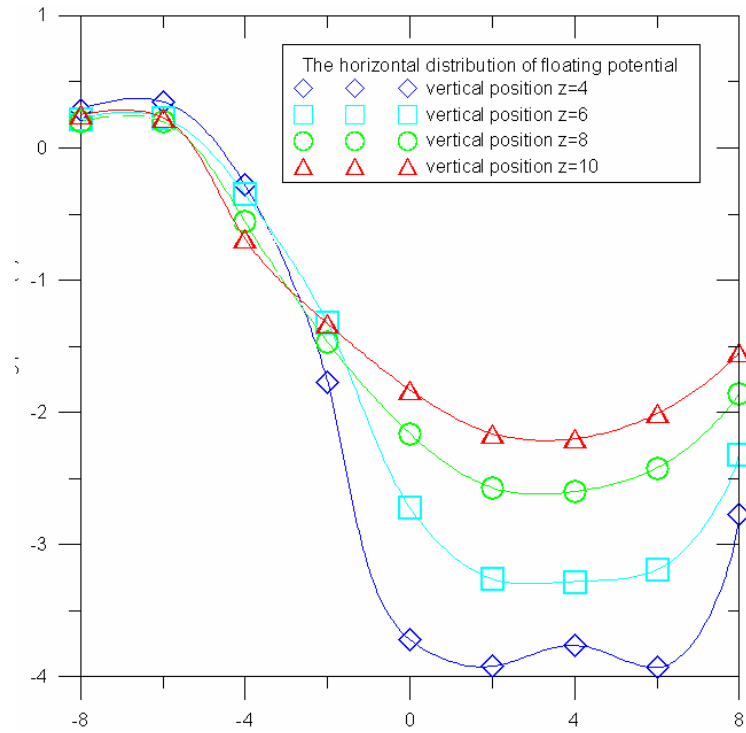
(a)



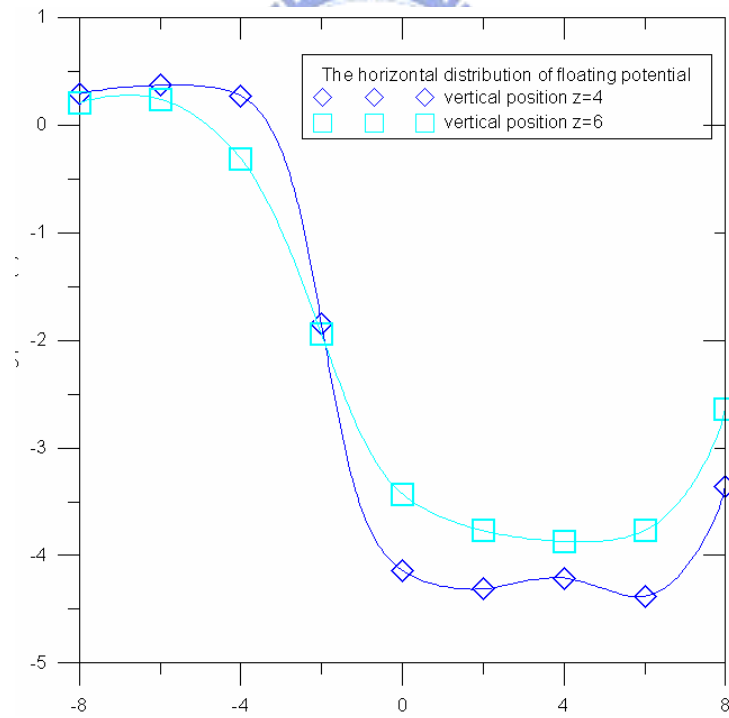
(b)

Figure 4.7. The horizontal distribution of floating potential in the pressure 20 mtorr and the distance between substrate and target is (a) 11 cm and (b) 8

cm.

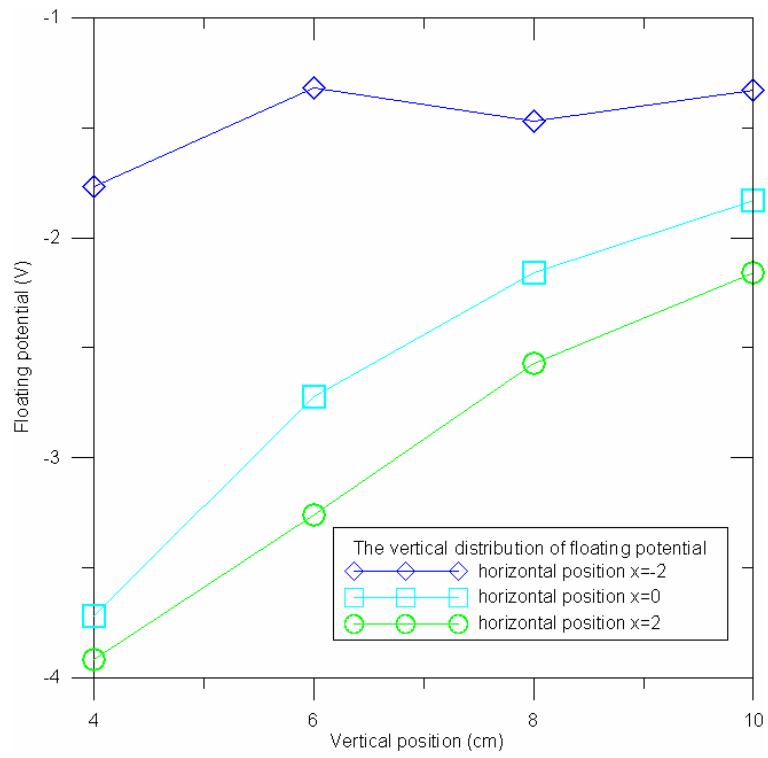


(a)

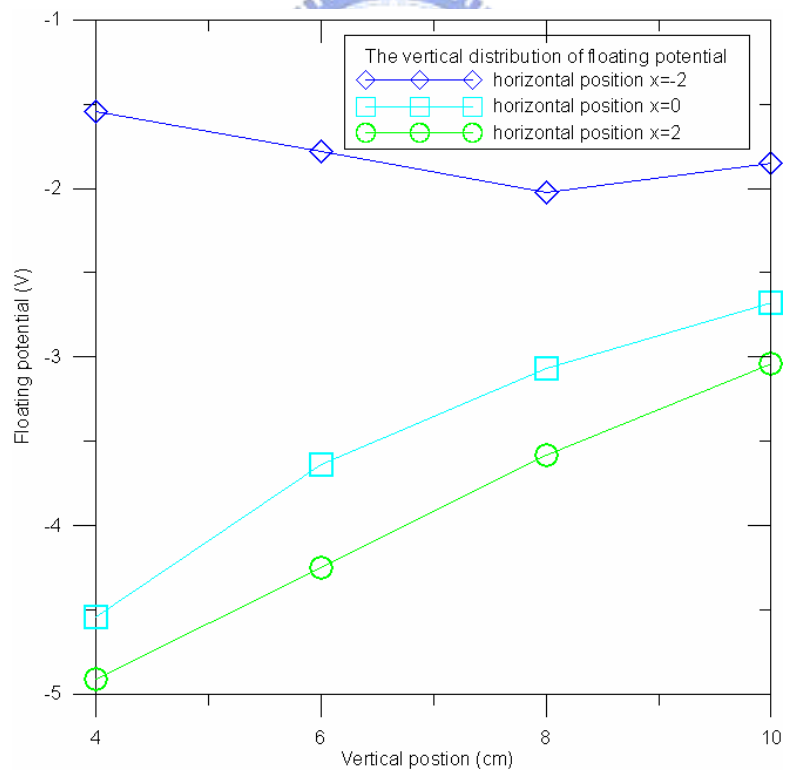


(b)

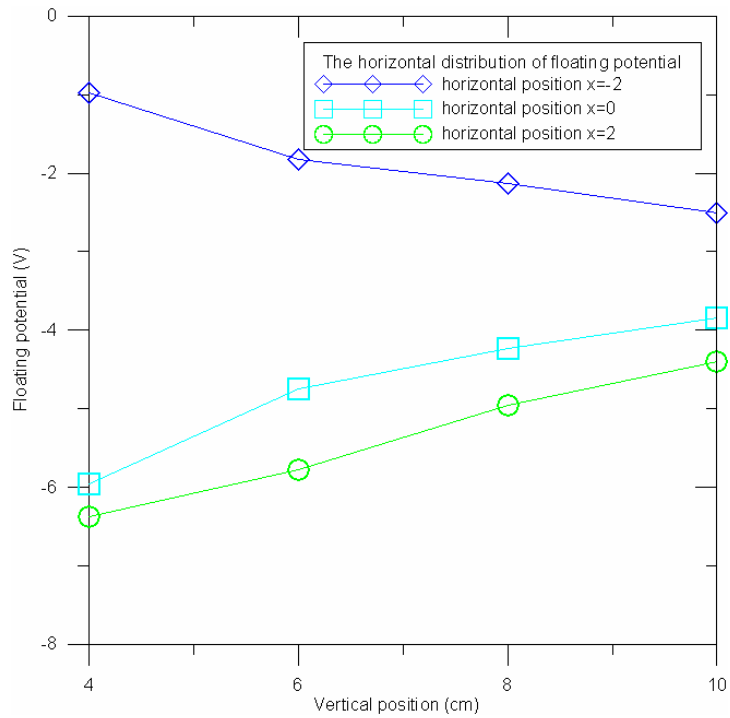
Figure 4.8. The horizontal distribution of floating potential in the pressure 30 mtorr and the distance between substrate and target is (a) 11 cm and (b) 8 cm.



(a)

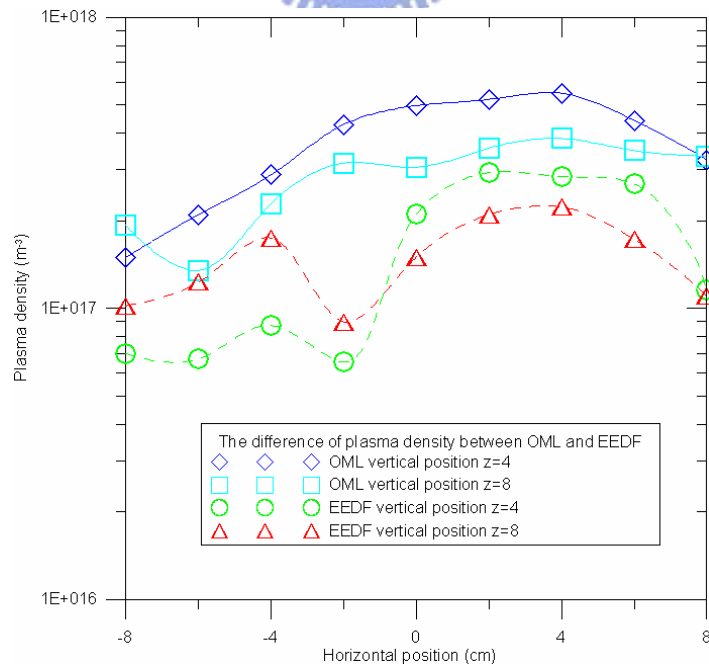
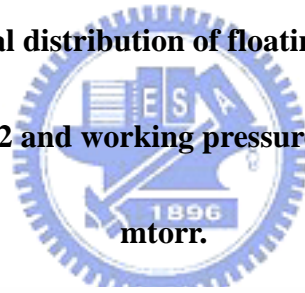


(b)

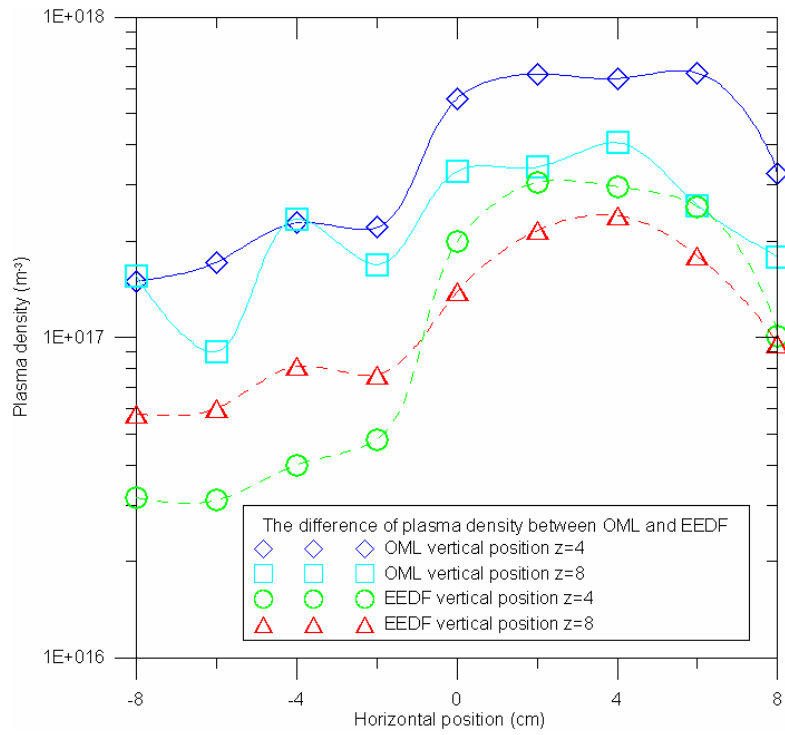


(c)

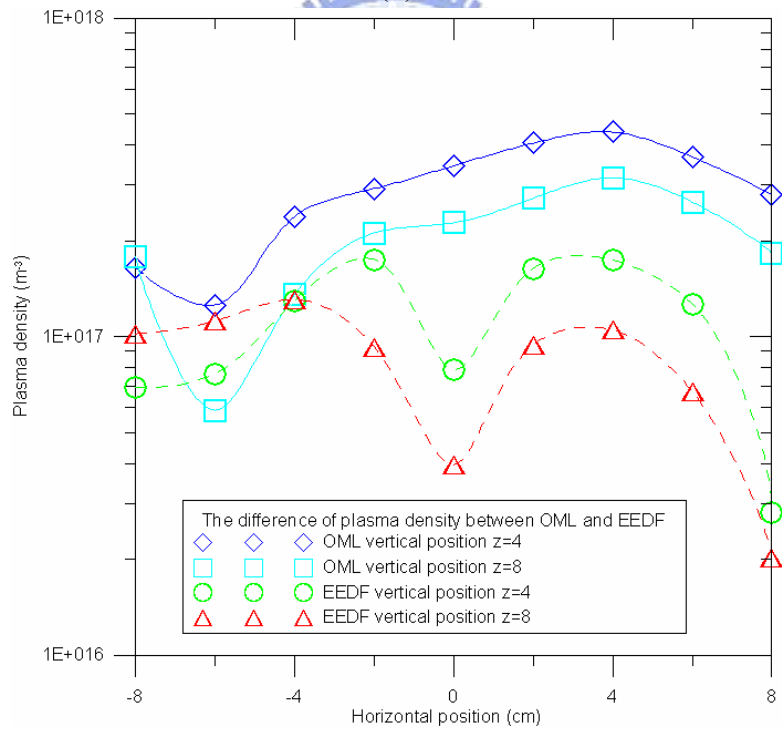
Figure 4.9. The vertical distribution of floating potential in the horizontal position $x=-2$, $x=0$ and $x=2$ and working pressure in (a) 30, (b) 20 and (c) 10 mtorr.



(a)

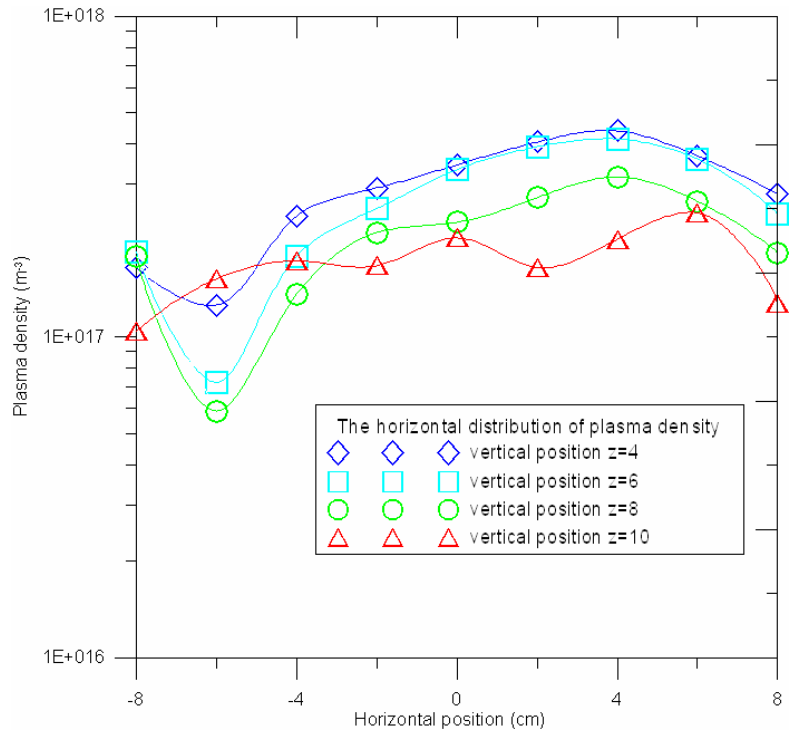


(b)

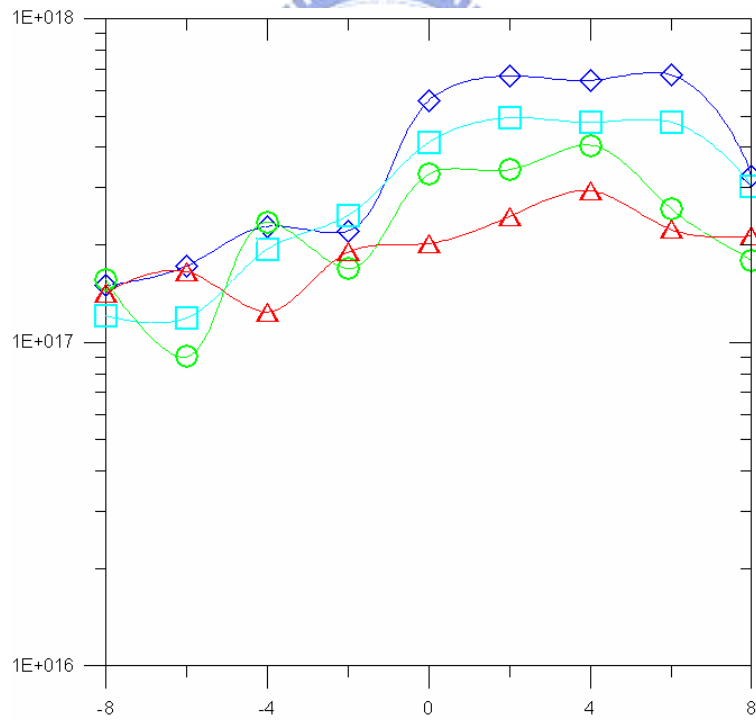


(c)

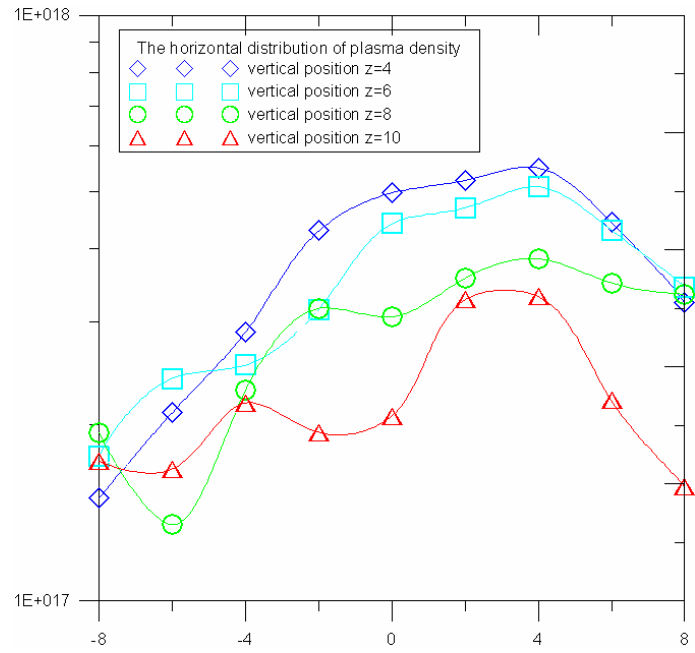
Figure 4.10. The difference of plasma density difference between *OML* and *EEDF*; the working pressure is (a) 30, (b) 20 and (c) 10 mtorr.



(a)

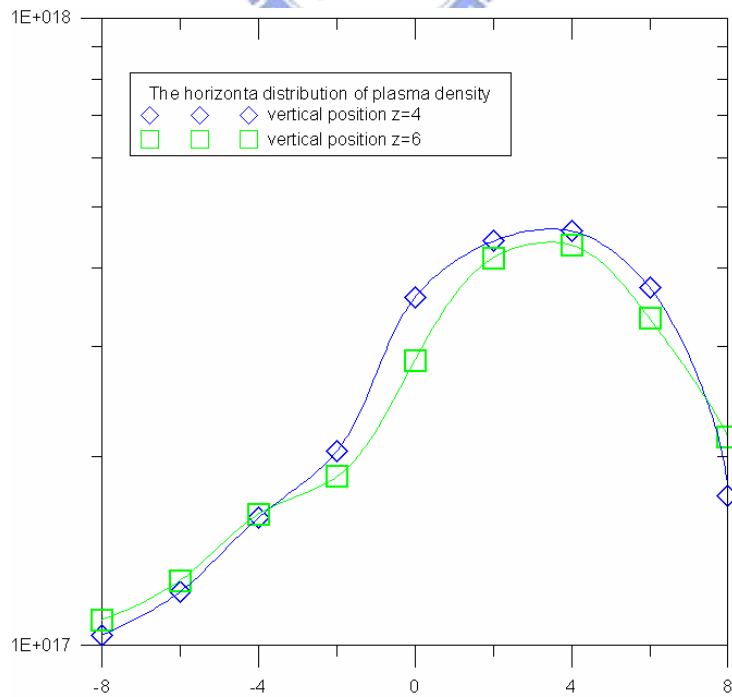


(b)

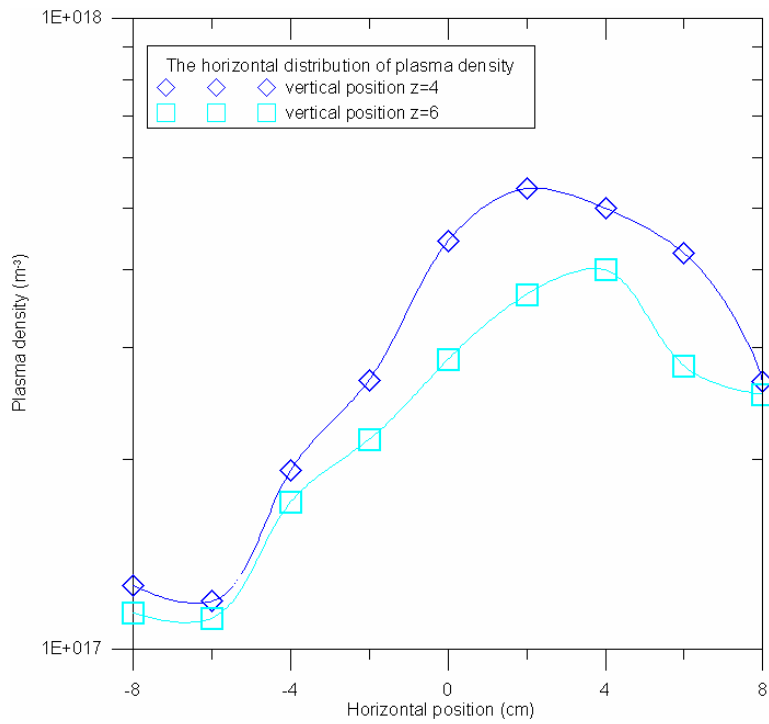


(c)

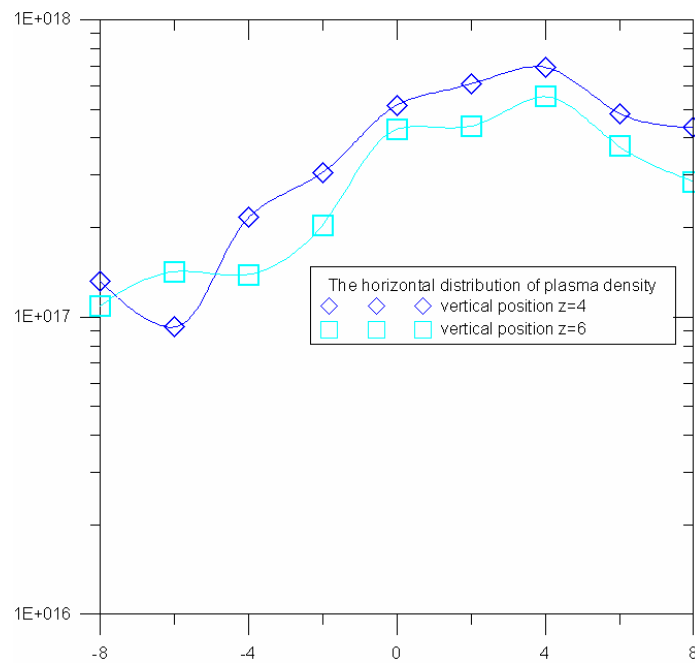
Figure 4.11. The horizontal distribution of plasma density in the distance 11 cm between the substrate and the target. The working pressure is (a) 10, (b) 20 and (c) 30 mtorr



(a)

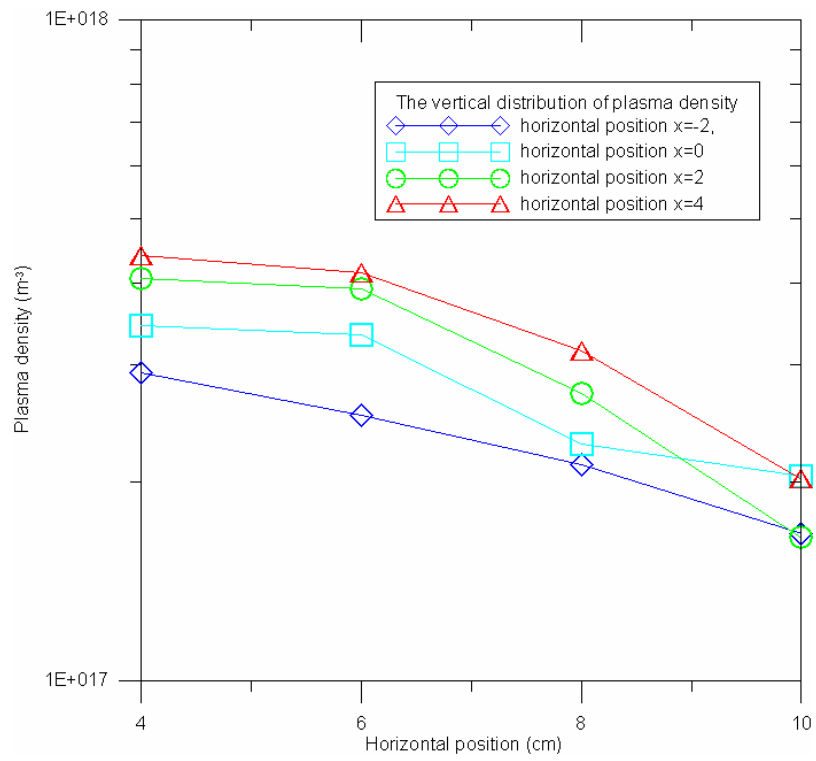


(b)

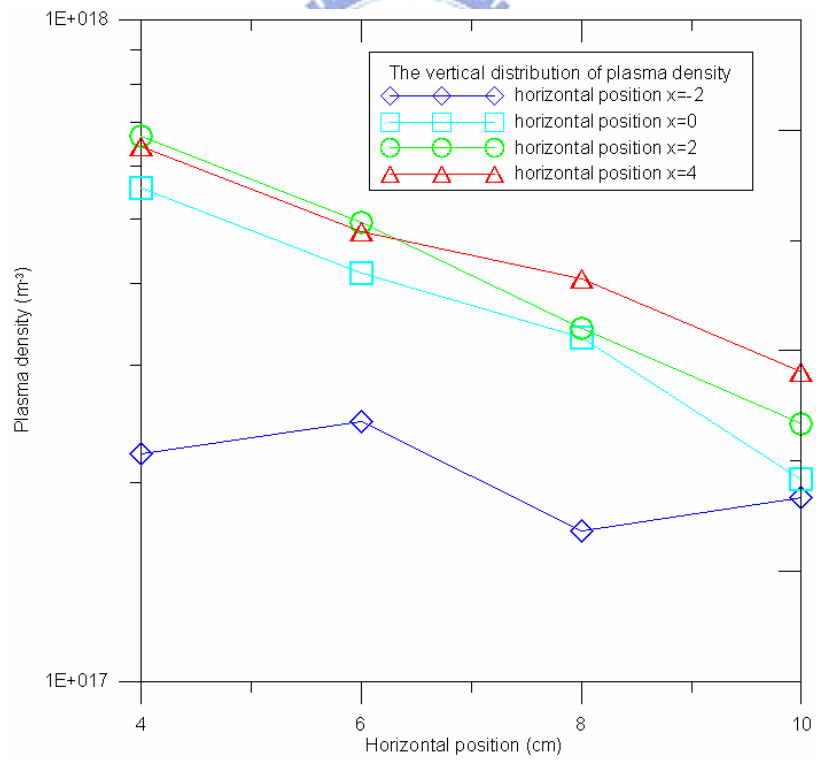


(c)

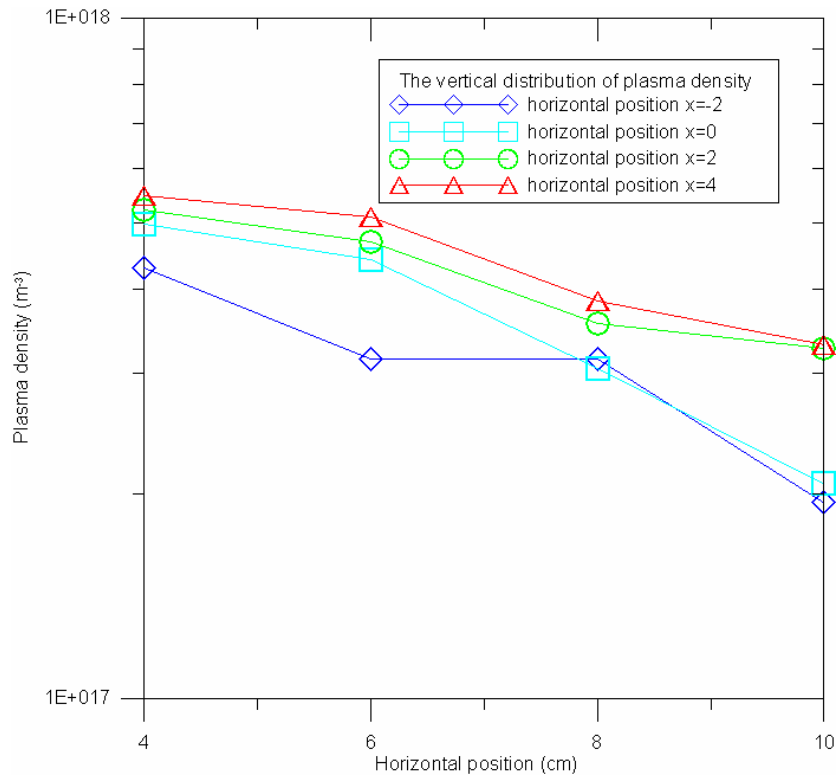
Figure 4.12. The horizontal distribution of plasma density in the distance 8 cm between the substrate and the target. The working pressure is (a) 10, (b) 20 and (c) 30 mtorr



(a)

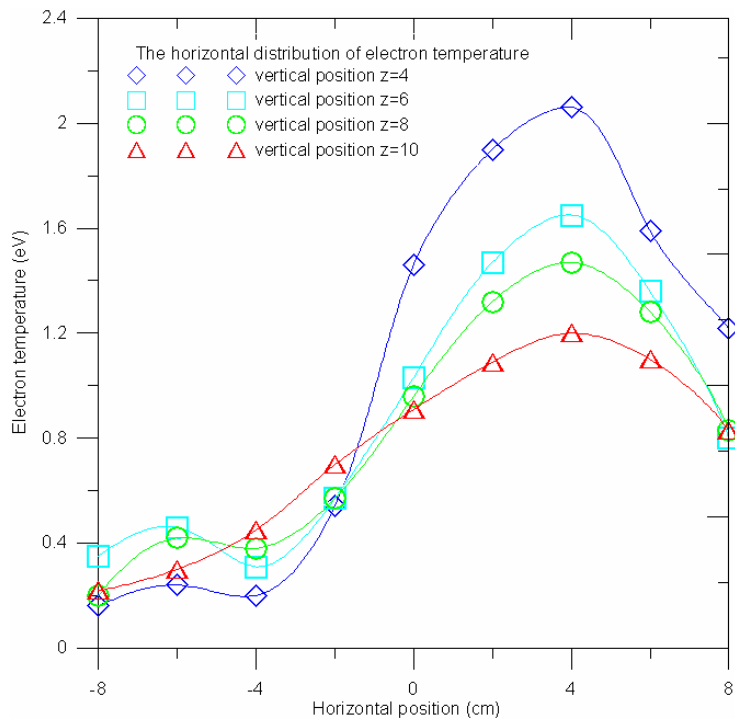


(b)



(c)

Figure 4.13. The vertical distribution of plasma density in the horizontal position $x=-2$, $x=0$, $x=2$ and $x=4$ and working pressure in (a) 10, (b) 20 and (c) 30 mtorr.



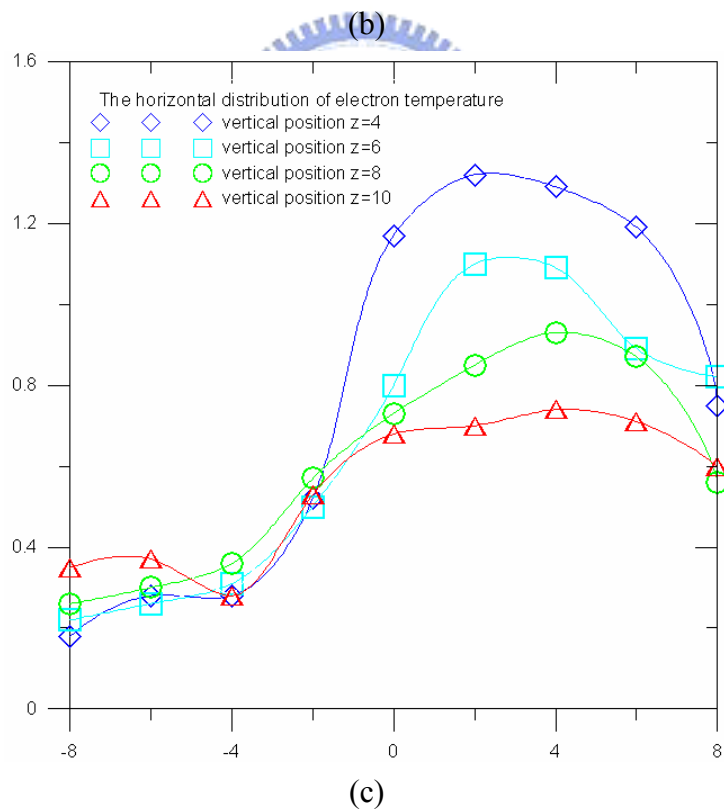
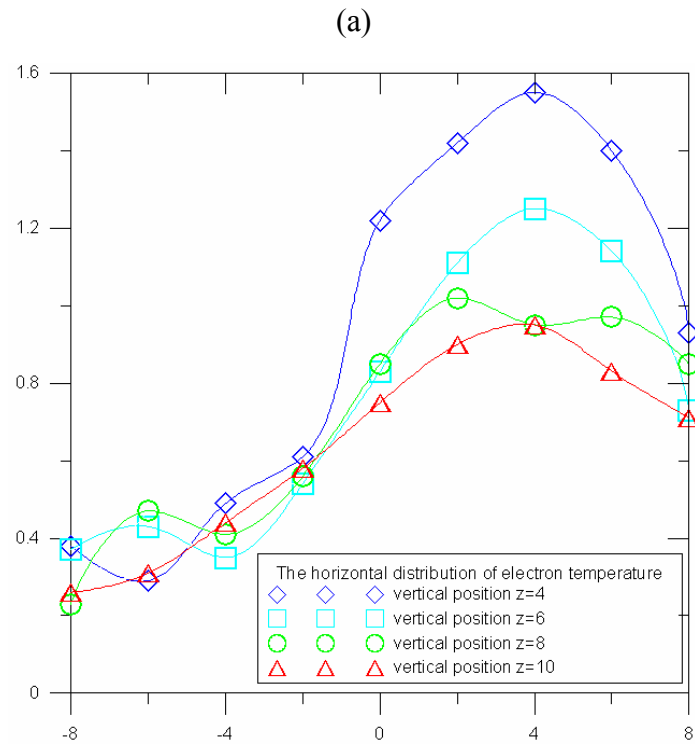
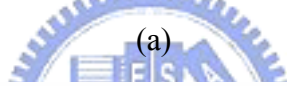
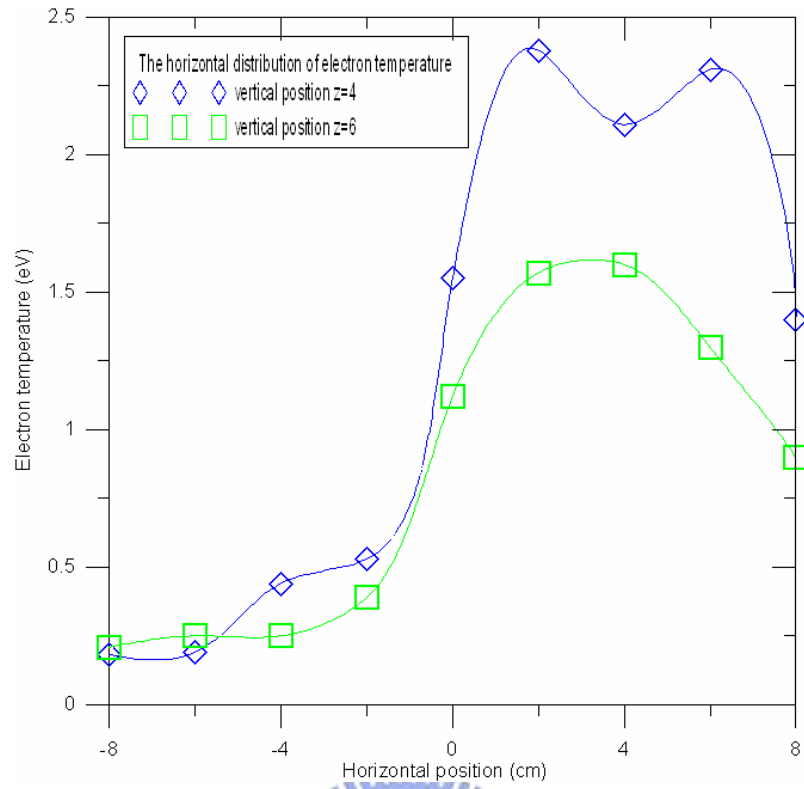
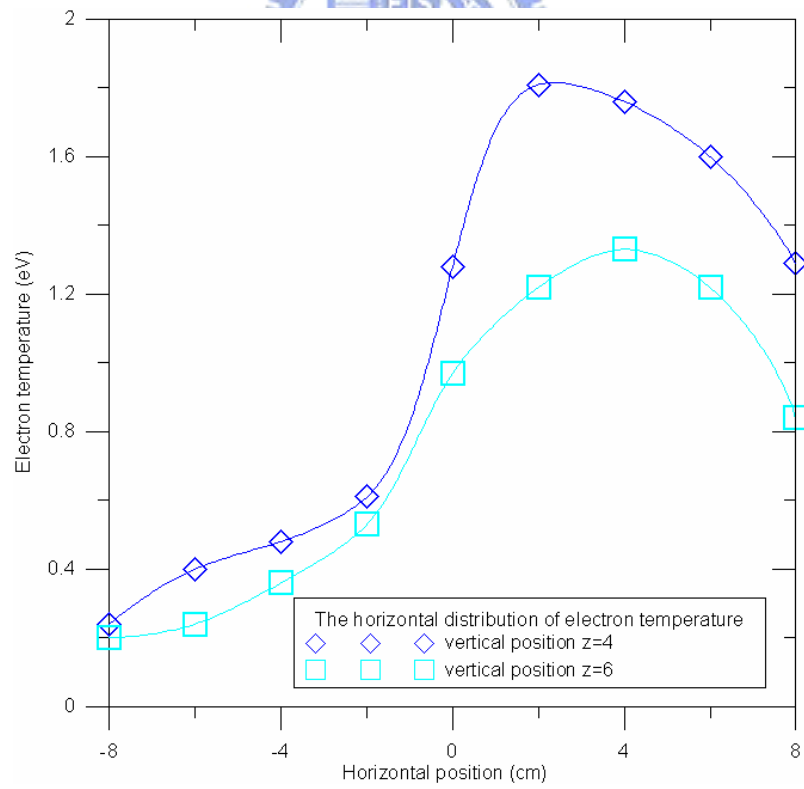


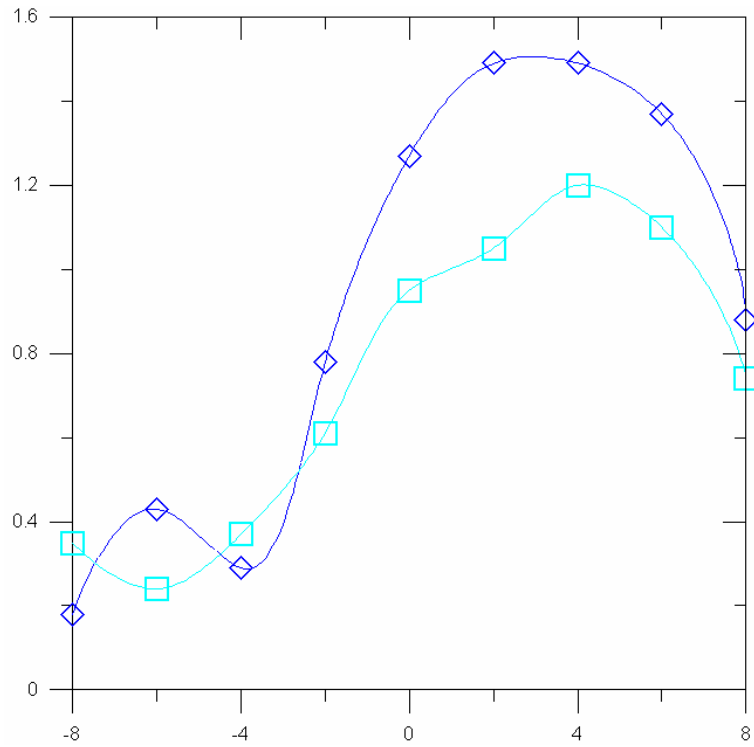
Figure 4.14. The horizontal distribution of electron temperature in the distance 11 cm between the substrate and the target. The working pressure is (a) 10, (b) 20 and (c) 30 mtorr



(a)

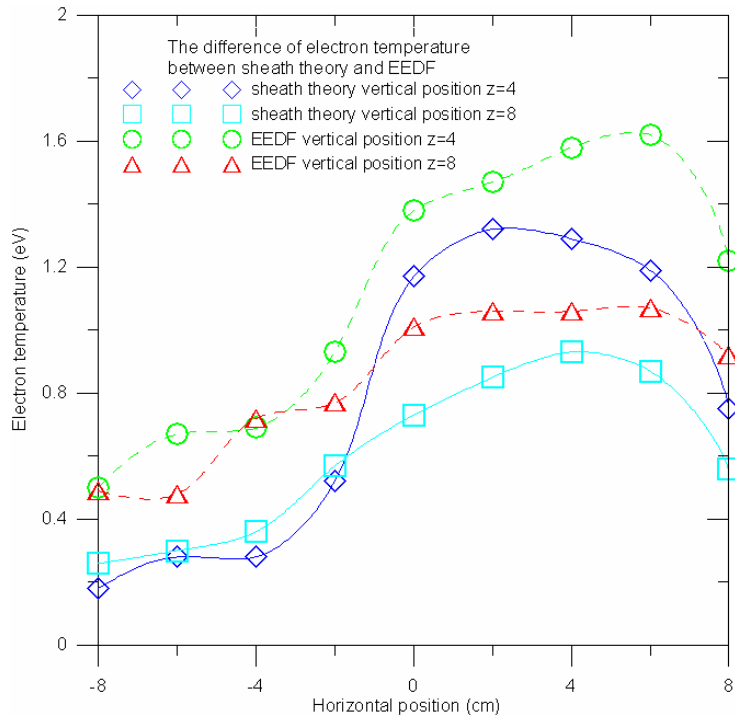


(b)

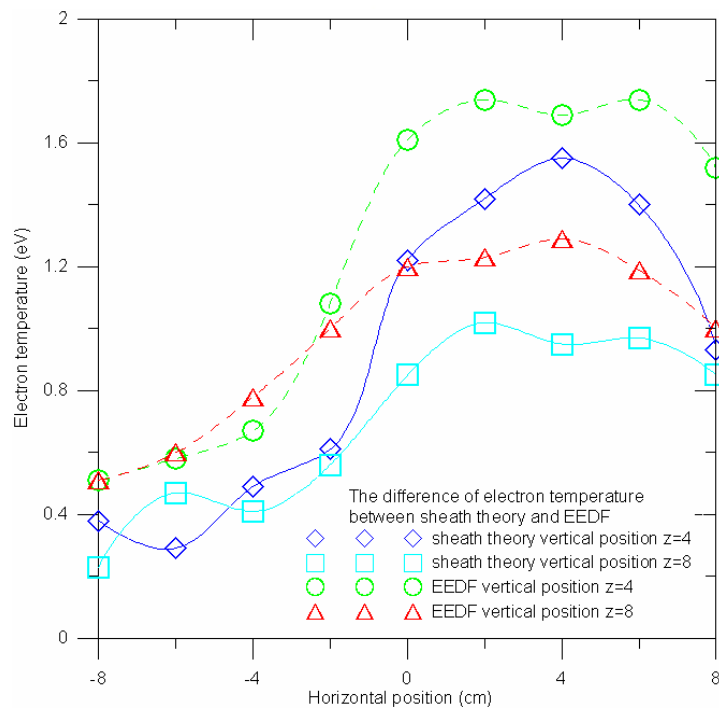


(c)

Figure 4.15. The horizontal distribution of electron temperature in the distance 8 cm between the substrate and the target. The working pressure is (a) 10, (b) 20 and (c) 30 mtorr

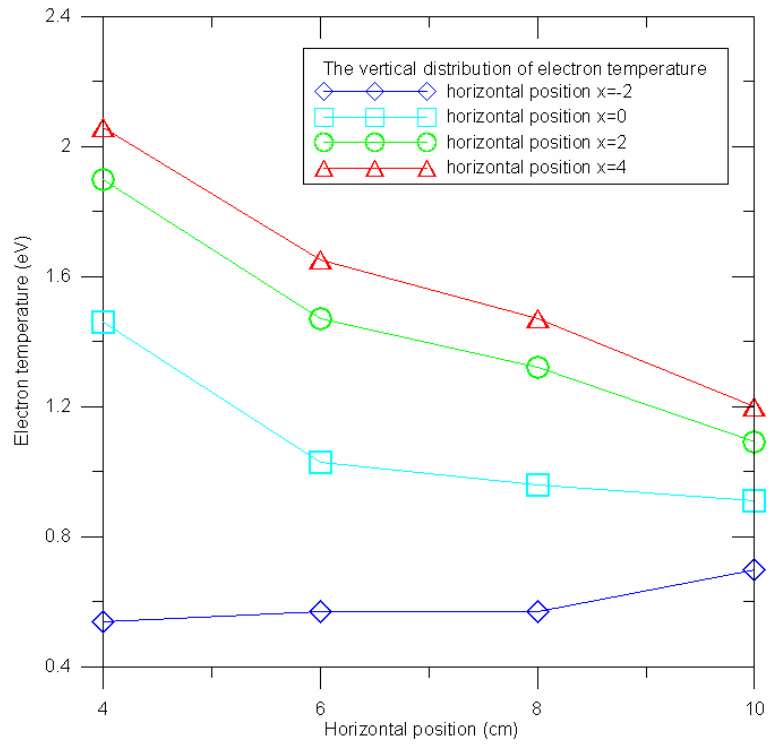


(a)

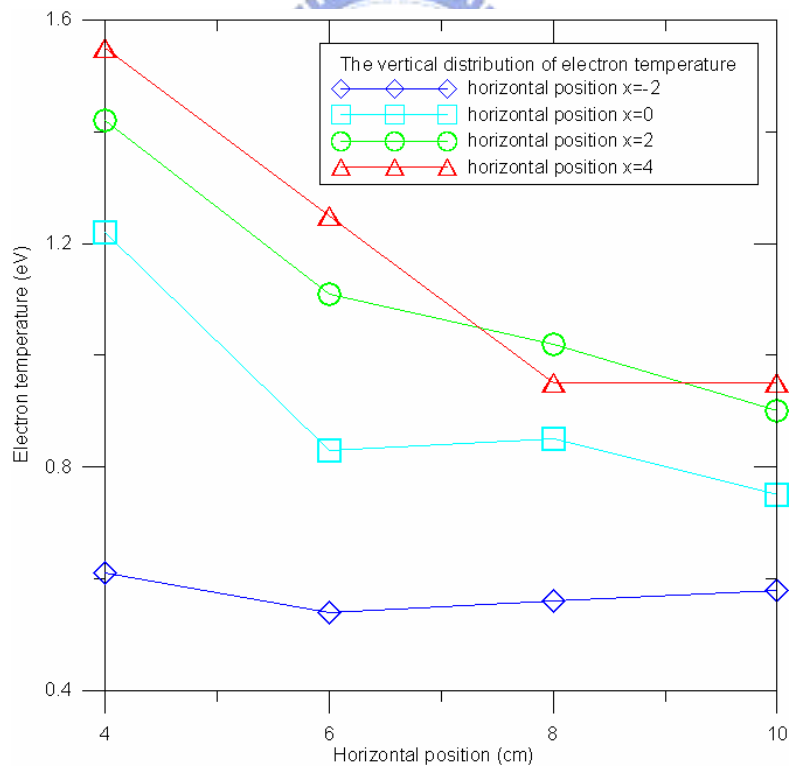


(b)

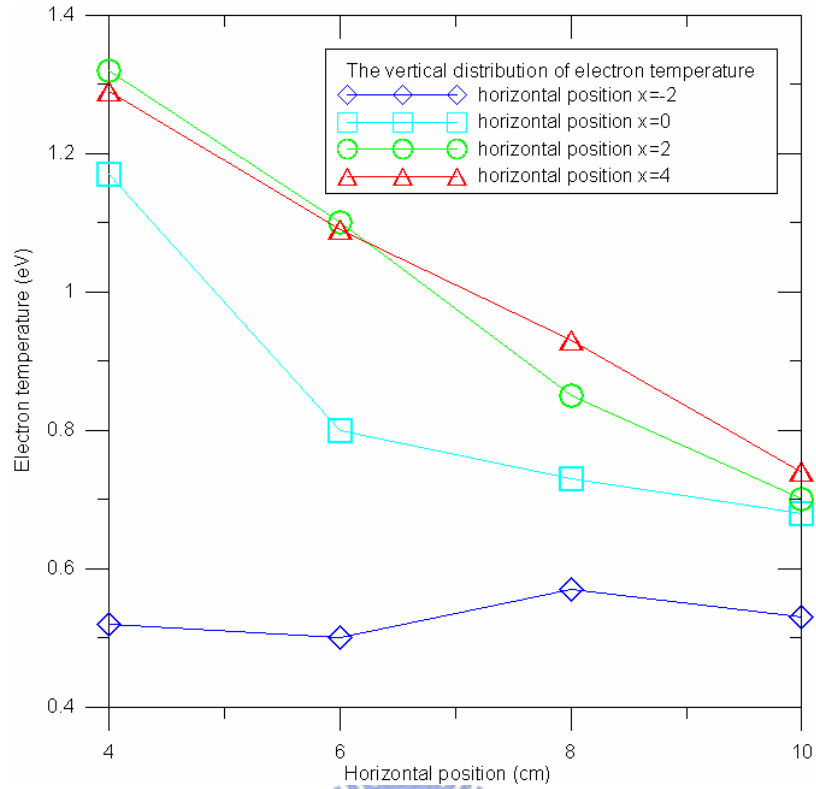
Figure 4.16. The difference of electron temperature between sheath theory and EEDF; the working pressure is (a) 30 and (b) 20 mtorr.



(a)



(b)



(c)

Figure 4.17. The vertical distribution of electron temperature in the horizontal position $x=-2$, $x=0$, $x=2$ and $x=4$ and working pressure in (a) 10, (b) 20 and (c) 30 mtorr.

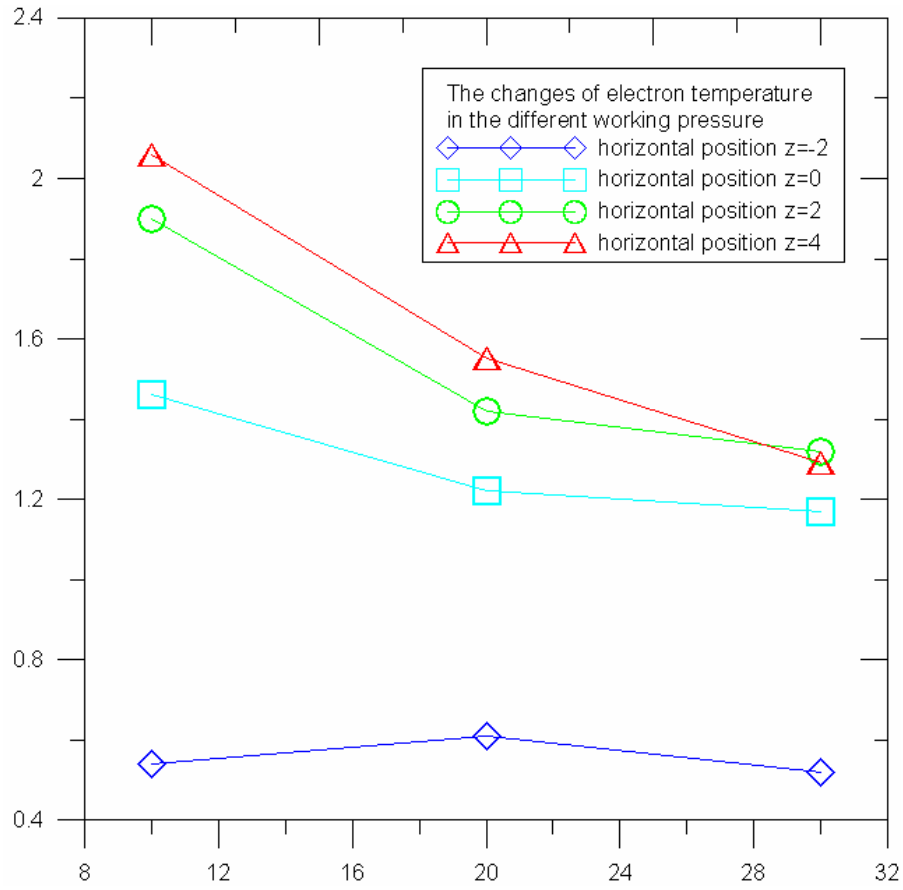
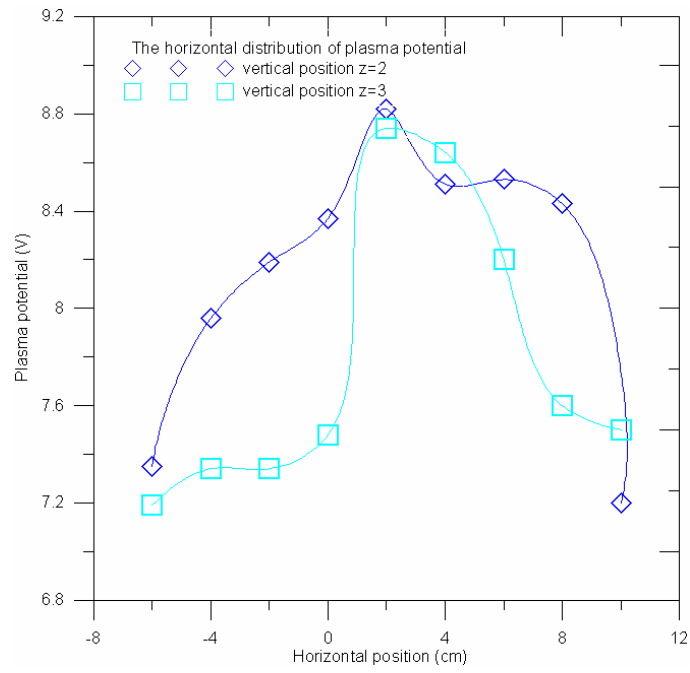


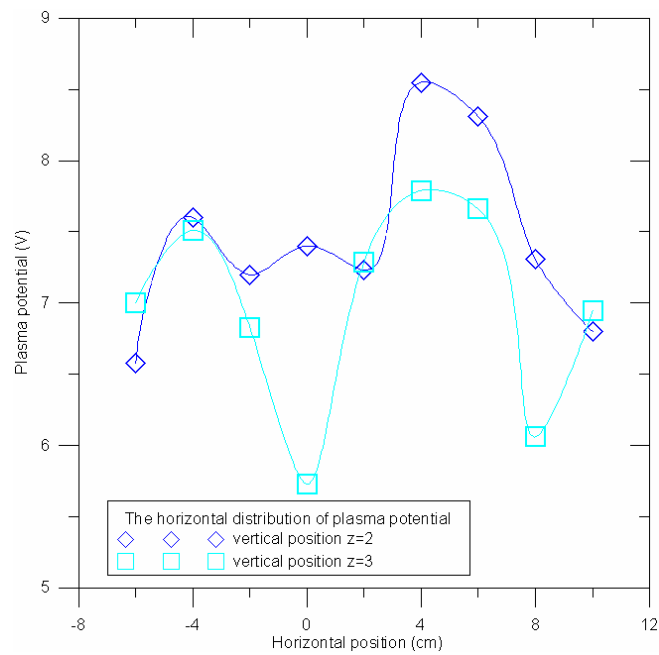
Figure 4.18. The changes of electron temperature in the different working pressure and in the same vertical position $z=4$



**Figure 4.19. The discharge was operated without the magnetron assembly in
the pressure 90 mtorr**

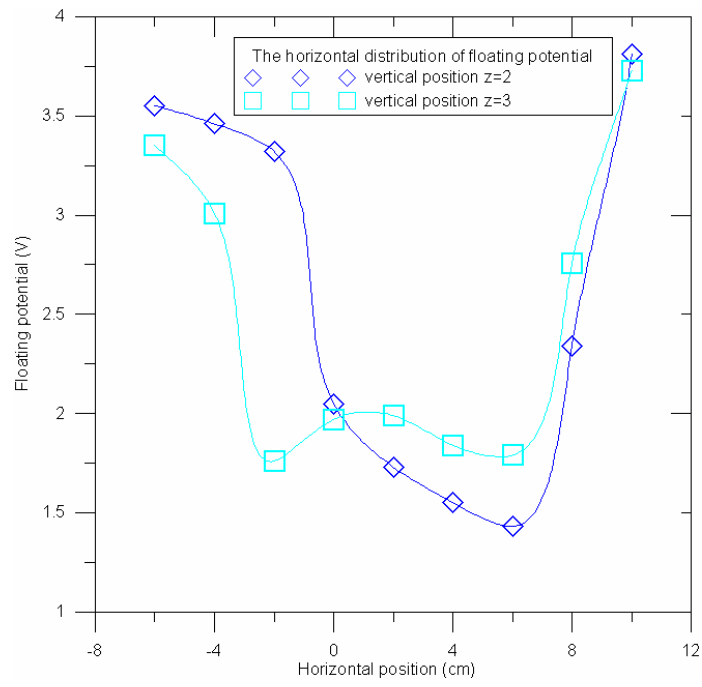


(a)

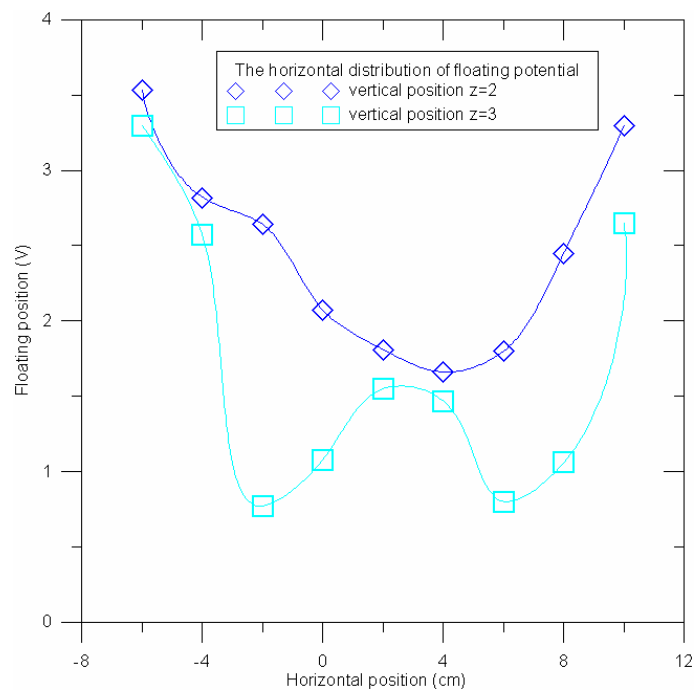


(b)

Figure 4.20. The horizontal distribution of plasma potential in the distance between substrate and target is 4 cm and working pressure (a) 70 mtorr and (b) 80 mtorr.

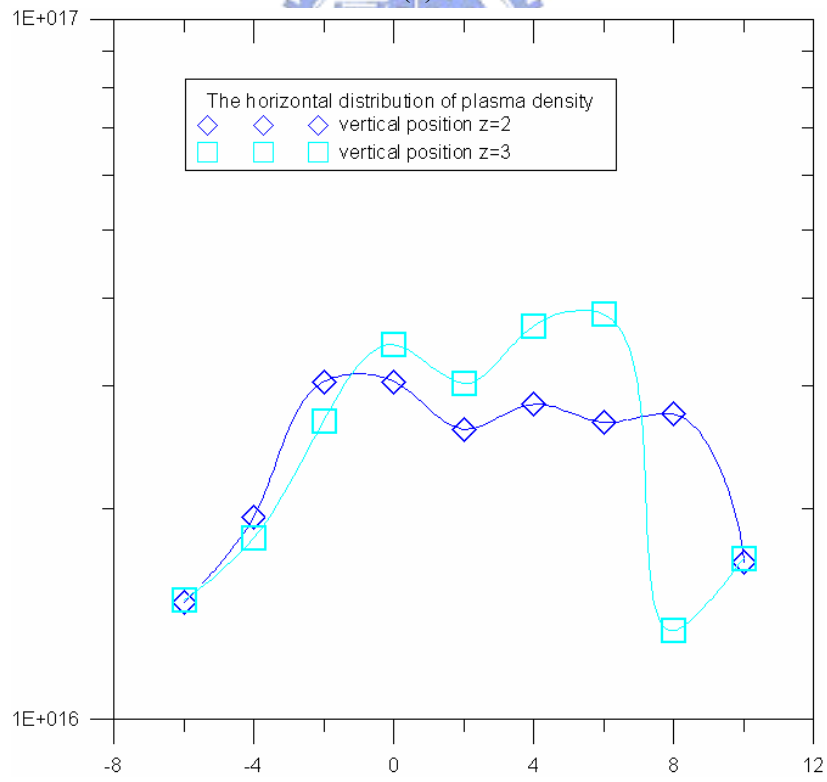
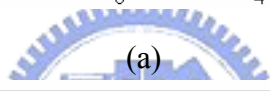
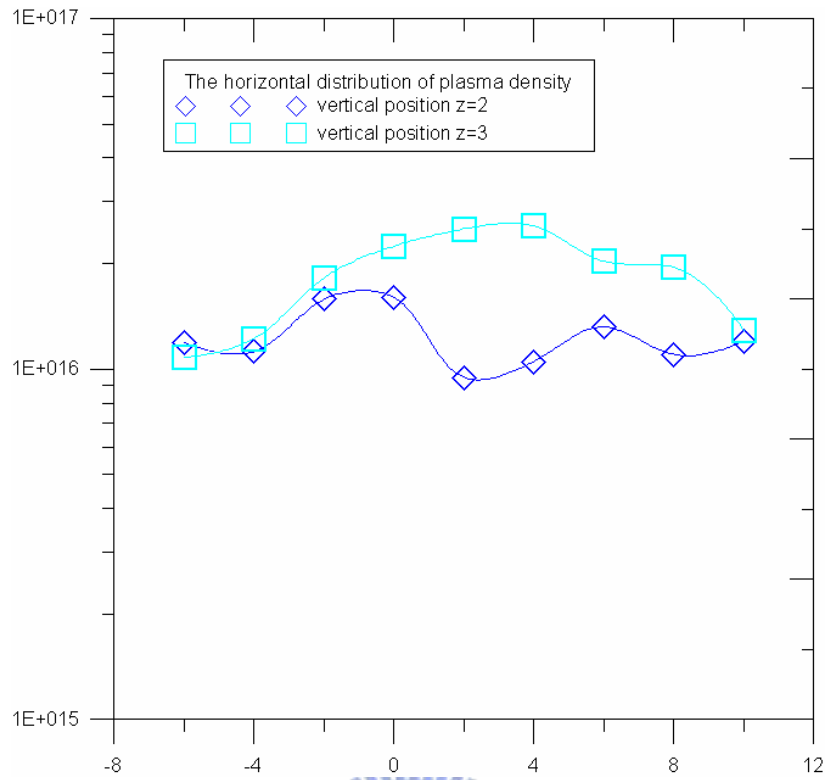


(a)

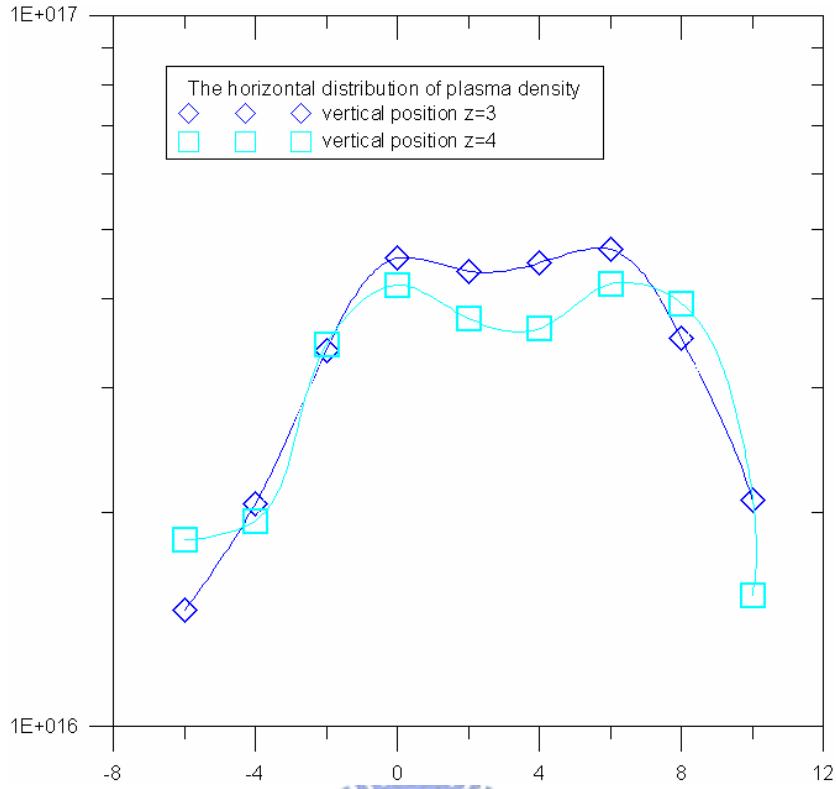


(b)

Figure 4.21. The horizontal distribution of floating potential in the distance between substrate and target is 4 cm and working pressure (a) 70 mtorr and (b) 80 mtorr.

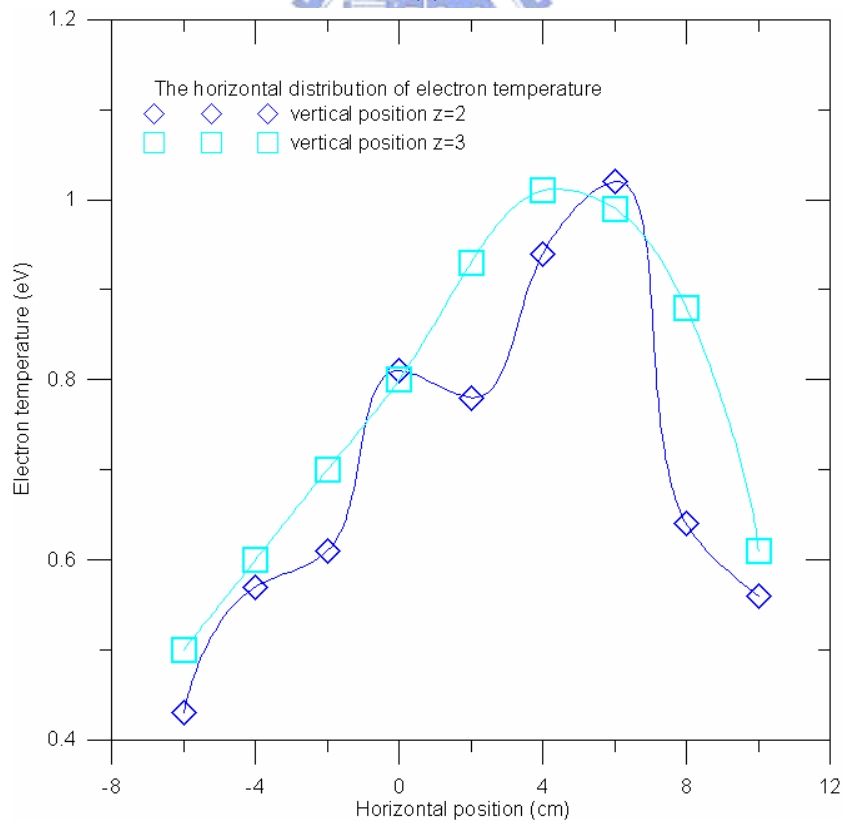
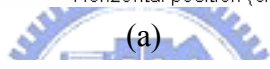
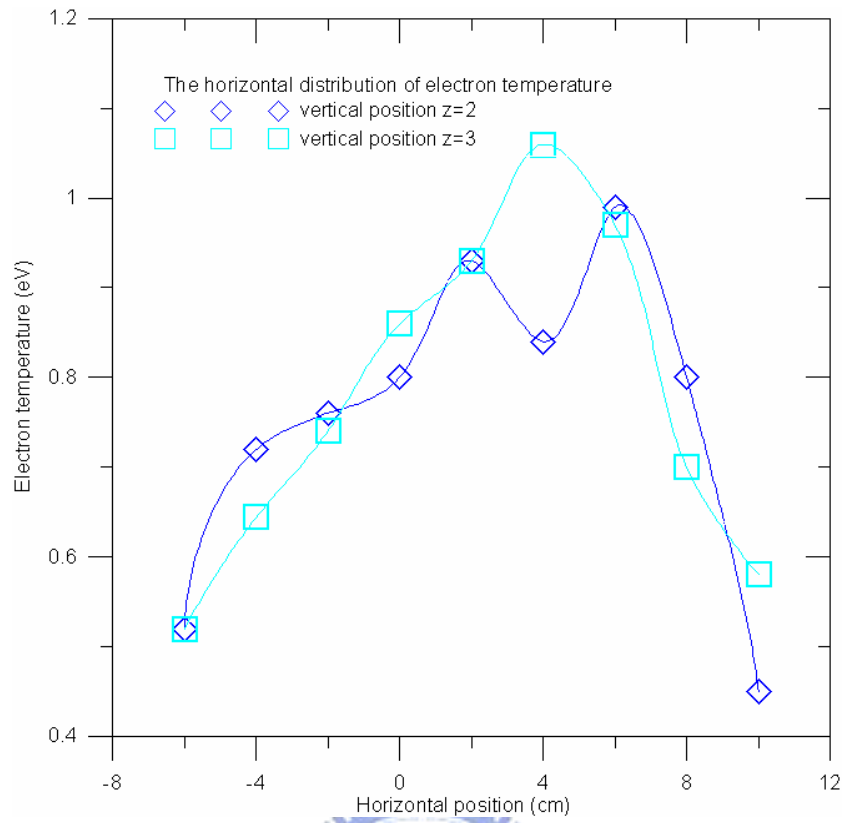


(b)

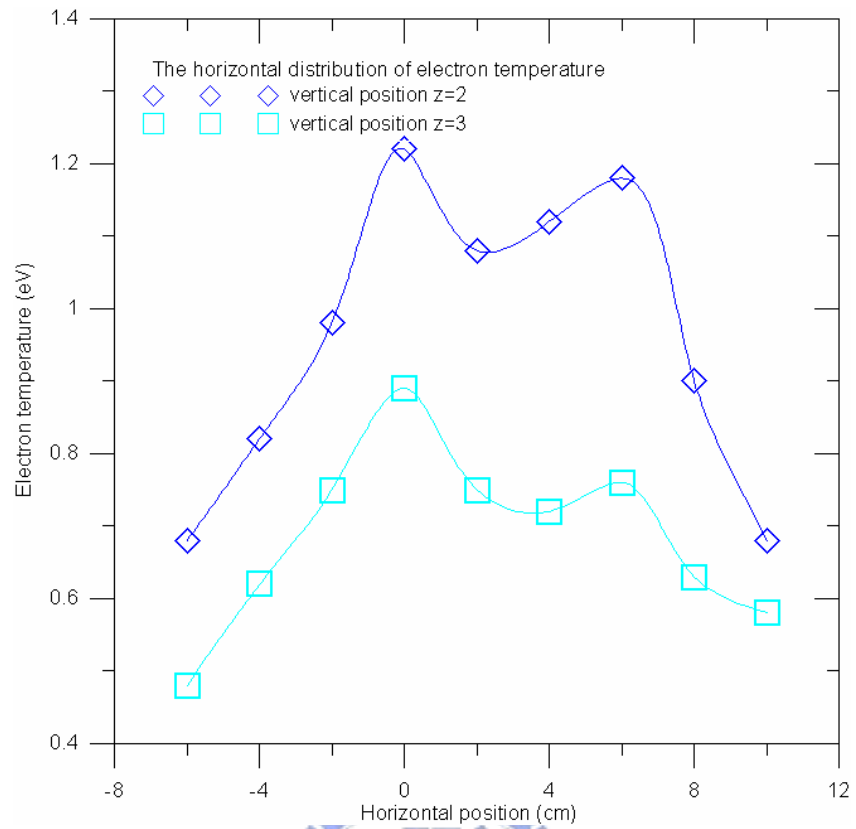


(c)

Figure 4.22. The horizontal distribution of plasma density in the distance between substrate and target is 4 cm at working pressure (a) 70 mtorr and (b) 80 mtorr and (c) the distance between substrate and target is 5 cm at working pressure 70 mtorr.



(b)



(c)

Figure 4.23. The horizontal distribution of electron temperature in the distance between substrate and target is 4 cm at working pressure (a) 70 mtorr and (b) 80 mtorr and (c) the distance between substrate and target is 5 cm at working pressure 70 mtorr.

Table 1. The value of $(V_p - V_f)/T_e$ in different places in the chamber with working pressure 30 mtorr and operated with magnetron

	z=4	z=6	z=8	z=10
x=-4	4.607315	3.897764	4.392265	5.531915
x=-2	5.387597	4.710579	4.78185	4.689266
x=-0	4.384615	4.91206	4.577657	4.449339
x=-2	4.030303	4.136364	4.310954	4.623044
x=-4	3.75969	4.110092	4.142395	4.519621
x=-6	4.168067	4.847458	4.209919	4.564607
x=-8	5.112882	4.613497	5.28777	4.504202



Table 2. The value of $(V_p - V_f)/T_e$ in different places in the chamber with working pressure 20 mtorr and operated with magnetron

	z=4	z=6	z=8	z=10
x=-2	3.861378	4.127706	3.743842	3.896396
x=0	3.943894	5.009208	5.420394	4.810997
x=-2	4.655738	5.457831	4.770318	4.745989
x=-4	4.105634	4.684685	4.480392	4.481605
x=-6	3.587097	4.16	4.658254	4.384858
x=-8	4.057143	4.473684	4.747162	4.564165
x=-10	4.962487	5.627586	4.799528	4.48519

Table 3. The value of $(V_p - V_f)/T_e$ in different places in the chamber with working pressure 10 mtorr and operated with magnetron

	z=4	z=6	z=8	z=10
x=-2	3.252788	4.761062	4.699647	4.871429
x=-0	4.726027	5.669903	5.460251	5.428571
x=-2	3.863158	4.707483	4.5	4.862385
x=-4	3.412621	4.533333	3.62585	4.35
x=-6	4.446541	4.926471	4.21875	4.8
x=-8	3.754098	6.318408	5.107914	5.283474



Table 4. The value of $(V_p - V_f)/T_e$ in different places in the chamber with working pressure 70 mtorr and operated without magnetron

	z=2	z=3
x=-6	7.307692	7.384615
x=-4	6.25	6.723602
x=-2	6.407895	7.540541
x=-0	7.9	6.406977
x=-2	7.623656	7.258065
x=-4	8.285714	6.415094
x=-6	7.171717	6.608247
x=-8	7.6125	6.914286
x=-10	7.533333	6.5

Table 5. The value of $(V_p - V_f)/T_e$ in different places in the chamber with working pressure 80 mtorr and operated without magnetron

	z=2	z=3
x=-6	7.093023	7.4
x=-4	8.385965	8.233333
x=-2	7.47541	8.657143
x=0	6.580247	5.8125
x=-2	6.948718	6.172043
x=-4	7.329787	6.257426
x=-6	6.382353	6.929293
x=-8	7.59375	5.681818
x=-10	6.25	7.04918



